MacLeod, C.J., Dick, H.J.B., Blum, P., and the Expedition 360 Scientists
Proceedings of the International Ocean Discovery Program Volume 360
publications.iodp.org

doi:10.14379/iodp.proc.360.101.2017

Expedition 360 summary[1]

H.J.B. Dick, C.J. MacLeod, P. Blum, N. Abe, D.K. Blackman, J.A. Bowles, M.J. Cheadle, K. Cho, J. Ciążela, J.R. Deans, V.P. Edgcomb, C. Ferrando, L. France, B. Ghosh, B.M. Ildefonse, M.A. Kendrick, J.H. Koepke, J.A.M. Leong, C. Liu, Q. Ma, T. Morishita, A. Morris, J.H. Natland, T. Nozaka, O. Pluemper, A. Sanfilippo, J.B. Sylvan, M.A. Tivey, R. Tribuzio, and L.G.F. Viegas[2]

Keywords: International Ocean Discovery Program, IODP, *JOIDES Resolution*, Expedition 360, Site U1473, Hole 1105A, Moho, Mohorovičić discontinuity, Southwest Indian Ridge, SloMo, Atlantis Bank, mid-ocean ridge, slow spreading rate, Atlantis II Transform, Hole 735B, Site U1309

Contents

Abstract

International Ocean Discovery Program (IODP) Expedition 360 was the first leg of Phase I of the SloMo (shorthand for "The nature of the lower crust and Moho at slower spreading ridges") Project, a multiphase drilling program that proposes to drill through the outermost of the global seismic velocity discontinuities, the Mohorovičić seismic discontinuity (Moho). The Moho corresponds to a compressional wave velocity increase, typically at ~7 km beneath the oceans, and has generally been regarded as the boundary between crust and mantle. An alternative model, that the Moho is a hydration front in the mantle, has recently gained credence upon the discovery of abundant partially serpentinized peridotite on the seafloor and on the walls of fracture zones, such as at Atlantis Bank, an 11–13 My old elevated oceanic core complex massif adjacent to the Atlantis II Transform on the Southwest Indian Ridge.

Hole U1473A was drilled on the summit of Atlantis Bank during Expedition 360, 1–2 km away from two previous Ocean Drilling Program (ODP) holes: Hole 735B (drilled during ODP Leg 118 in 1987 and ODP Leg 176 in 1997) and Hole 1105A (drilled during ODP Leg 179 in 1998). A mantle peridotite/gabbro contact has been traced by dredging and diving along the transform wall for 40 km. The contact is located at ~4200 m depth on the transform wall below the drill sites but shoals considerably 20 km to the south, where it was observed in outcrop at 2563 m depth. Moho reflections, however, have been found at ~5–6 km beneath Atlantis Bank and <4 km beneath the transform wall, leading to the suggestion that the seismic discontinuity may not represent the crust/mantle boundary but rather an alteration (serpentinization) front. This in turn raises the interesting possibility that methanogenesis associated with serpentinization could support a whole new planetary biosphere deep in the oceanic basement. The SloMo Project seeks to test these hypotheses at Atlantis Bank and evaluate the processes of natural carbon sequestration in the lower crust and uppermost mantle.

A primary objective of SloMo Leg 1 was to explore the lateral variability of the stratigraphy established in Hole 735B. Comparison of Hole U1473A with Holes 735B and 1105A allows us to demonstrate a continuity of process and complex interplay of magmatic accretion and steady-state detachment faulting over a time period of ~128 ky. Preliminary assessment indicates that these sections of lower crust are constructed by repeated cycles of intrusion, represented in Hole U1473A by approximately three upwardly differentiated hundreds of meter–scale bodies of olivine gabbro broadly similar to those encountered in the deeper parts of Hole 735B.

Specific aims of Expedition 360 focused on gaining an understanding of how magmatism and tectonism interact in accommodating seafloor spreading, how magnetic reversal boundaries are expressed in the lower crust, assessing the role of the lower crust and shallow mantle in the global carbon cycle, and constraining the extent and nature of life at deep levels within the ocean lithosphere.

Summary

International Ocean Discovery Program (IODP) Expedition 360 was the first leg of Phase I of the SloMo (shorthand for "The nature of the lower crust and Moho at slower spreading ridges") Project, a multiphase drilling program that proposes to drill through the outermost of the global seismic velocity discontinuities, the Mohorovičić seismic discontinuity (Moho). The Moho corresponds to a compressional wave velocity increase from ~6.7 km/s to between 7.6 and 8.6 km/s, typically at ~7 km beneath the oceans. Since the work of Adams and Coker (1906), Adams and Williamson (1923), and Wrinch and Jeffreys (1923), the Moho has generally been regarded as the boundary between crust and mantle; however, an al-

[1] Dick, H.J.B., MacLeod, C.J., Blum, P., Abe, N., Blackman, D.K., Bowles, J.A., Cheadle, M.J., Cho, K., Ciążela, J., Deans, J.R., Edgcomb, V.P., Ferrando, C., France, L., Ghosh, B., Ildefonse, B.M., Kendrick, M.A., Koepke, J.H., Leong, J.A.M., Liu, C., Ma, Q., Morishita, T., Morris, A., Natland, J.H., Nozaka, T., Pluemper, O., Sanfilippo, A., Sylvan, J.B., Tivey, M.A., Tribuzio, R., and Viegas, L.G.F., 2017. Expedition 360 summary. *In* MacLeod, C.J., Dick, H.J.B., Blum, P., and the Expedition 360 Scientists, *Southwest Indian Ridge Lower Crust and Moho*. Proceedings of the International Ocean Discovery Program, 360: College Station, TX (International Ocean Discovery Program). http://dx.doi.org/10.14379/iodp.proc.360.101.2017

[2] **Expedition 360 Scientists' addresses.**

MS 360-101: Published 30 January 2017

ternative model, that the Moho is a hydration front in the mantle (Hess, 1960, 1962), has recently gained credence upon the discovery of abundant partially serpentinized peridotite on the seafloor and on the walls of fracture zones. One such location is Atlantis Bank, an 11–13 My old elevated oceanic core complex massif adjacent to the Atlantis II Transform on the Southwest Indian Ridge (SWIR).

IODP Hole U1473A was drilled on the summit of Atlantis Bank during Expedition 360, 1–2 km away from two previous Ocean Drilling Program (ODP) holes: Hole 735B (drilled during ODP Leg 118 in 1987 and ODP Leg 176 in 1997) and Hole 1105A (ODP Leg 179 in 1998). A mantle peridotite/gabbro contact has been traced for 15 km at ~4200 m depth along the transform wall ~11.5 km to the west. Moho reflections have, however, been found at ~5–6 km beneath Atlantis Bank, leading to the suggestion that the seismic discontinuity may not represent the crust/mantle boundary but rather an alteration (serpentinization) front (Muller et al., 2000). This in turn raises the interesting possibility that methanogenesis associated with serpentinization could support a whole new planetary biosphere deep in the oceanic basement. The SloMo Project seeks to test these hypotheses at Atlantis Bank and evaluate the processes of natural carbon sequestration in the lower crust and uppermost mantle.

Located on the north-central part of Atlantis Bank, 2.2 km north-northeast of Hole 735B, Hole U1473A was drilled 789.7 m drilling depth below seafloor (DSF) into massive gabbro cut by isolated dikes. The shallower part of the hole has been affected by faulting: in the upper 469 m, seven distinct fault systems were encountered, ranging from 5 cm thick cataclasite bands to a 50 m thick carbonate-veined chlorite-rich fault zone. Over this interval, we obtained 44% recovery under relatively poor drilling conditions. From 469 m DSF to the bottom of the hole, however, drilling conditions were excellent, similar to Hole 735B, with 96% recovery in the lowermost 212 m interval cored (577.5–789.7 m DSF). Hole U1473A is the deepest hole ever drilled from the seafloor into ocean crust during a single 2 month expedition. The hole is in good condition overall and, after minor remediation operations carried out during IODP Expedition 362T (July 2016), can be reoccupied.

A primary objective of SloMo Leg 1 was to explore the lateral variability of the stratigraphy established in Hole 735B. Comparison of Hole U1473A with Holes 735B (Dick et al., 2000) and 1105A (Casey et al., 2007) allows us to demonstrate a continuity of process and complex interplay of magmatic accretion and steady-state detachment faulting over a time period of ~128 ky. Preliminary assessment indicates that these sections of lower crust are constructed by repeated cycles of intrusion, represented in Hole U1473A by approximately three upwardly differentiated hundreds of meter–scale bodies of olivine gabbro broadly similar to those encountered in the deeper parts (>500 meters below seafloor [mbsf]) of Hole 735B.

The gabbro bodies in Hole U1473A are transposed by intense locally pervasive ductile deformation, with extensive intervals of sheared porphyroclastic to ultramylonitic gabbro (often Fe-Ti oxide rich) forming a 600 m thick crystal-plastic shear zone. Notably, shear sense is both normal and reversed in the upper section of the hole but predominantly reversed in the lower part. Similar relationships are also seen in Hole 735B; all are probably a response of the Atlantis Bank oceanic core complex to flexure during exhumation. Deformation is noticeably less intense toward the bottom of Hole U1473A, with primary subophitic igneous textures often well preserved in the lowermost 200 m. Overall, the presence of such extensive crystal-plastic deformation in Hole U1473A and elsewhere at Atlantis Bank demonstrates that magmatic accretion took place in a highly dynamic environment, beginning while the gabbros were partially molten and continuing as they cooled and were exhumed tectonically from beneath the rift valley floor.

The average composition for Hole U1473A is very similar to Hole 735B, with Mg# of 71 and 0.7 wt% TiO_2. However, H_2O contents averaging 1.0 wt%, even in petrographically fresh samples, are much higher than expected for pristine gabbro cumulates. Most of the gabbros drilled in Hole U1473A are olivine gabbro, with lesser but still significant proportions of gabbro and oxide-bearing gabbro. The relationship between these rock types is complex and ranges from simple interlocking igneous contacts between undeformed gabbros with subparallel coarse to pegmatitic oxide gabbro layers, to isolated patches of oxide- and pyroxene-rich gabbro intercalated with the olivine gabbro, to oxide concentrations that indicate local migration of late Fe-Ti oxide–rich melts along active shear zones. The Fe-Ti–rich oxide gabbro and gabbronorite occurrences, whether in layers and patches or within shear zones, appear to have crystallized from evolved interstitial melt compacted out of the olivine gabbro cumulates and record the migration of these melts through the section. Evidence for percolation of more primitive melts through the section is also ubiquitous, with fine-grained microgabbros intruding or replacing the coarse olivine gabbro. Approximately 1.5% of the section consists of late magmatic felsic veins ranging in composition from diorite to trondhjemite. These may represent the final stages of fractionation of the melts intruded to form the gabbros or may instead be produced by reheating and partial anatexis of the section by successive intrusive events. Several diabase dikes intruded gabbros that had been altered under conditions ranging from granulite to greenschist facies. These include granoblastic hornblende diabase dikes that appear to have partially melted the crystal-plastically deformed gabbro host to form trondhjemite. Overall, the bulk of the gabbros are too fractionated to be in equilibrium with the mid-ocean-ridge basalt (MORB) exposed on the hanging wall (e.g., Natland et al., 1991; Robinson et al., 1996) and scattered over the detachment fault surface, reflecting a complex evolution beyond initial intrusion of basaltic melt.

The Hole U1473A section has undergone static hydrothermal alteration, extensive recrystallization associated with crystal-plastic deformation, and alteration associated with veining and with late cataclastic deformation. Static alteration occurs throughout the hole, ranging from <3% to 90%, with locally intense veining and characterized by colorless amphibole, talc, serpentine, and clay minerals after olivine; however, away from fault zones, much of the section is very fresh (78% with <30% replacement minerals). Formation of near-ubiquitous brown hornblende and secondary clinopyroxene reflect near-solidus conditions, whereas other assemblages reflect amphibolite to sub-greenschist facies. Clay minerals are the last alteration products, reflecting temperatures <150°C. Amphibolite facies alteration and overprinting clay mineral formation are significant largely at shallow depths, whereas intervals displaying greenschist facies alteration are found sporadically throughout the hole. Carbonate with or without clay and oxidative reddish clay replacement of olivine is also more conspicuous in intervals disturbed by faulting, whereas deeper in the hole micro veins filled with chlorite, with or without amphibole, are more typical.

Felsic veins in Hole U1473A often have high abundances of secondary sulfides and clay minerals as well as replacement of primary plagioclase by albitic and occasionally secondary quartz, showing that these were pathways for large volumes of hydrothermal fluids. This observation was also made for Hole 735B. A key similarity between Holes U1473A, 735B, and 1105A is the occurrence of amphi-

bole veins, which is largely limited to the shallower sections of the holes.

Specific objectives of SloMo Leg 1 included drilling through a magnetic reversal that was projected to lie several hundred meters below seafloor at Site U1473: from reversely polarized at the surface to normally polarized at depth. Virtually all intervals drilled in Hole U1473A have positive inclinations, indicating, in the Southern Hemisphere, a reversed polarity magnetization that places the hole within geomagnetic polarity Chron C5r.3r, as in Hole 735B. Magnetizations are sufficient to account for the observed sea-surface anomalies at Atlantis Bank. A clear reversal boundary was not reached during Expedition 360; however, thermal demagnetization revealed characteristic remanence with negative inclination (normal polarity) in narrow altered intervals in the lower part of the hole, leading us to suggest that we are entering a reversal transition near the bottom of Hole U1473A. Three intervals with statistically significant differences in inclination downhole may document differential block rotations due to faulting.

Background and objectives

Expedition 360 constituted the first leg of the multiphase SloMo Project that aims ultimately to drill through the Moho seismic discontinuity at Atlantis Bank at the ultraslow-spreading SWIR (Figure **F1**). By penetrating this fundamental seismological boundary, the SloMo Project will test the hypothesis that the Moho, at least at slow- and ultraslow-spreading ridges, represents an alteration boundary such as the lower limit of mantle lithosphere serpentinization rather than the igneous crust–mantle transition (Figure **F2**). If the latter, the igneous crust/mantle boundary could lie at any depth above the seismic boundary.

The site chosen for this deep drill hole is Atlantis Bank, an elevated flat-topped massif at ~700 m water depth on the east flank of the north-south–trending Atlantis II Transform (Figures **F1**, **F3**) (Dick et al., 1991b). The Moho here lies at ~5.5 km below the platform summit (Figure **F4**) (Muller et al., 2000). The principal aim of Expedition 360 was to drill as deep as possible through lower crustal gabbro and leave a hole open and ready to be deepened during subsequent expeditions. A target depth of 1300 mbsf was originally estimated, derived from prior experience of drilling conditions at Atlantis Bank and assuming a nominal 4 days contingency time for weather and operational issues; however, this depth was not achieved largely because the number of days available for coring during Expedition 360 was substantially less than planned (see **Operations** in the Site U1473 chapter [MacLeod et al., 2017b]).

On the basis of local geological knowledge from site survey investigations, it was thought unlikely that the igneous crust/mantle boundary would be encountered or a significant amount of peridotite recovered during Expedition 360 itself. The aim of future SloMo expeditions is to reoccupy and deepen the hole with the overall goal of penetrating the crust–mantle transition, which is believed to be as much as ~2.5 km above the Moho (see below). Additional drilling, potentially using the riser D/V *Chikyu*, is likely to be necessary to penetrate the Moho itself at ~5 km below seafloor (Figure **F4**).

The SloMo Project is not simply focused on the ultimate goal of drilling the crust/mantle boundary; equally important is what we learn on each step of the journey on the way there. By recovering a substantial section of the igneous lower crust at Atlantis Bank, Expedition 360 was designed to address specific key challenges set out in the IODP Science Plan 2013–2023 (**http://www.iodp.org/about-iodp/iodp-science-plan-2013-2023**). This document, representing the consensus of the global ocean drilling community, posits that in order to understand the inherent connections between the Earth's interior and its surface environment we must address fundamental questions about basic plate tectonic processes. Central among these questions are how seafloor spreading and mantle melting lead to the creation of oceanic lithosphere at mid-ocean ridges,

Figure F1. 3-D perspective view of the Atlantis II Transform, looking north-northeast. Data compiled from multibeam data collected during *Conrad* Cruise C2709, *James Clark Ross* Cruise JR31, *Yokosuka* and *Kairei* site survey cruises, and several French multibeam expeditions, combined with satellite gravity seafloor data and the Global Multi-Resolution Topography database (**http://www.marine-geo.org/portals/gmrt**) (see also Mendel et al., 1997, 2003; Dick et al., 1999; Kinoshita et al., 2001; Matsumoto et al., 2002; Sauter et al., 2004; Baines et al., 2007).

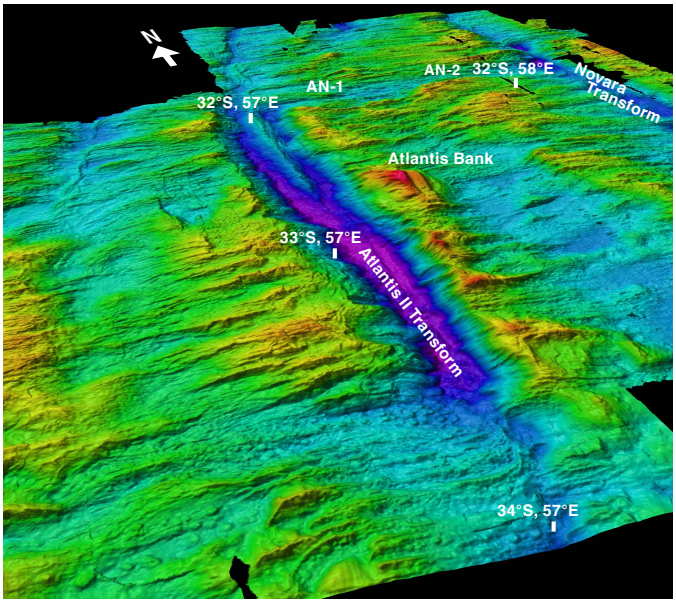

Figure F2. Alternative models for the lower crust and mantle (modified from Dick et al., 2006).

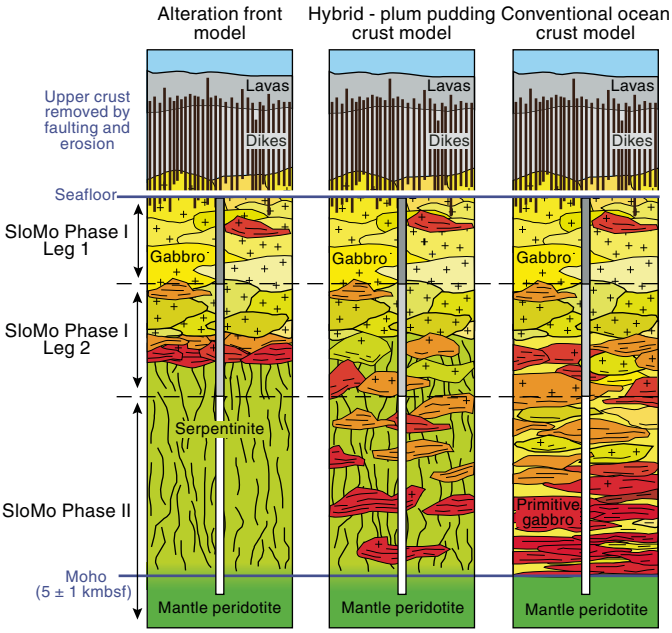

Figure F3. A. Bathymetry of Atlantis Bank area, with ODP/IODP drill sites marked. B. Summary of mapping of the same area, with geological interpretation by H.J.B. Dick based on site survey results (MacLeod et al., 1998; Kinoshita et al., 2001; Matsumoto et al., 2002).

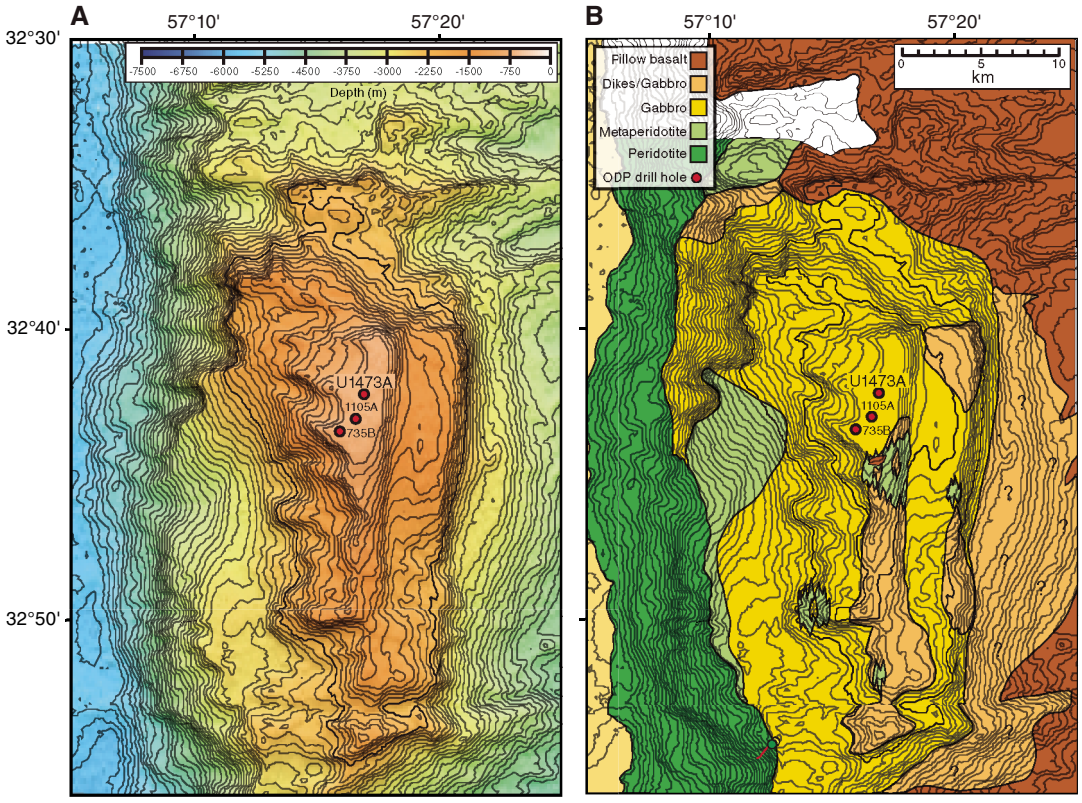

Figure F4. Velocity models for north–south seismic Line CAM101 over Atlantis Bank, together with principal drill sites (modified after Muller et al., 2000). Green line = depth of Hole U1473A drilled during Expedition 360, orange line = projected penetration during the remainder of SloMo Phase I, red line = projected penetration during SloMo Phase II (riser drilling). Velocity contours = 0.4 km/s. Upper panel shows an undifferentiated Layer 3; lower panel shows a lower serpentinized mantle Layer 3 and an upper gabbroic Layer 3. The models fit the data equally well. Triangles = ocean-bottom hydrophones. Hole U1473A lies on the line, Hole 735B is projected from a kilometer to the west. Moho gaps are due to ocean-bottom seismometer placement and are not real (R.S. White, pers. comm., 2000).

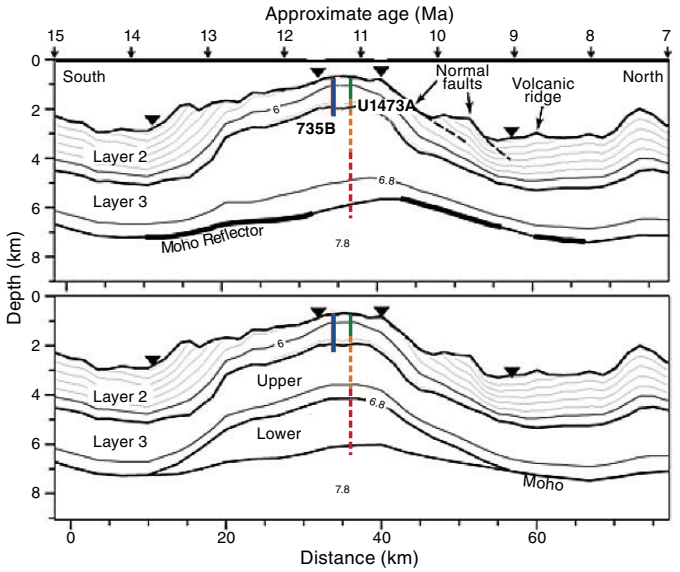

and what controls the architecture of the ocean crust thus formed (IODP Science Plan Challenge 9). Constraining the composition, diversity, and architecture of the lower ocean crust and shallow mantle is critical to understanding the global geochemical cycle, particularly the exchange of heat, mass, and volatiles between the Earth's interior, oceans, and atmosphere.

At slow- and ultraslow-spreading ridges, the lower crust uniquely preserves that critical link where magmatic and tectonic processes directly reflect plate dynamics, melt input, and the mantle flow pattern. We now know that at such ridges a substantial portion of plate spreading is accommodated in the lower crust by tectonic extension due to faulting and, in places, ductile deformation (e.g., Mutter and Karson, 1992). Large-offset "detachment" normal faults exert a strong control on melt distribution and transport in the lower crust and its delivery to the seafloor. This is in marked contrast to fast-spreading ridges, where it is accepted that the crust principally undergoes magmatic accretion by the injection of melt into the lower crust, diking, and eruption of magmas on the seafloor. Rollover and corner flow by ductile flow accompanying mantle upwelling and plate spreading is believed to be mostly limited to the mantle; however, at slower spreading ridges, which are cooler and support only ephemeral magma chambers, the lower crust can potentially support a shear stress. As a consequence, with lower rates of magma supply and colder, stronger lithosphere formed directly beneath the ridge axis, slower spreading ridges have very different morphologies and crustal architectures. Thus, as stated in IODP Initial Science Plan Challenge 9, a full picture of crustal architecture and accretion can only be drawn if both fast- and slow-spreading environments are investigated.

Specific aims of Expedition 360, the first leg of Phase I of the SloMo Project, therefore focused on gaining an understanding of how magmatism and tectonism interact in accommodating seafloor spreading, how magnetic reversal boundaries are expressed in the lower crust, assessing the role of the lower crust and shallow mantle in the global carbon cycle, and constraining the extent and nature of life at deep levels within the ocean lithosphere. These are explained further in **Scientific objectives** below.

Geological setting

With a full spreading rate of 14 mm/y the SWIR lies at the slow end of the mid-ocean-ridge spreading-rate spectrum. The ridge trends approximately southwest–northeast for most of its length. Between ~52°E and 60°E, the ridge spreads almost due north–south, and it is offset by a series of closely spaced large-offset transform faults. One of these, the Atlantis II Transform at 57°E (Fisher and Sclater, 1983), offsets the SWIR sinistrally by 200 km (Dick et al., 1991b) (Figure **F1**). Between this transform and the Novara Transform ~140 km to the east, the spreading axis is divided into two segments, AN-1 and AN-2, separated by a 17 km offset nontransform discontinuity at 57°40′E (Mendel et al., 1997; Hosford et al., 2003; Baines et al., 2007). The spreading rate here is asymmetric: at the short westerly Segment AN-1 adjacent to the northern ridge/transform intersection of the Atlantis II Transform, magnetic anomalies reveal rates of 8.5 mm/y to the south and 5.5 mm/y to the north, and the transform has been lengthening by 3 mm/y for at least the past 20 My (Dick et al., 1991b; Hosford et al., 2003; Baines et al., 2007). At ~20 Ma, a 10° counterclockwise change in regional spreading direction put the Atlantis II Transform into transtension for a period of ~12 My (Dick et al., 1991b, Hosford et al., 2003; Baines et al., 2007, 2008).

Immediately to the east of the Atlantis II Transform, parallel to it and on a flow line directly south of spreading Segment AN-1, is an elevated transverse ridge (Figure **F1**). It consists of a series of uplifted blocks connected by saddles that rise to as little as 700 meters below sea level (mbsl) (Dick et al., 1991b). Atlantis Bank (32°43′S, 57°17′E) forms the shallowest and northernmost portion of this ridge, 95 km south of the SWIR axis (Figures **F1**, **F3**). The bank consists of a raised dome ~40 km long by ~30 km wide, rising from 5700 mbsl at the base of the transform wall to 700 mbsl on a ~25 km² flat-topped wave-cut platform at its crest and then drops to 4300 mbsl on its eastern flank across two prominent transform-parallel east-dipping normal faults (Dick et al., 1991b; Baines et al., 2003; Hosford et al., 2003).

Site surveys of the Atlantis Bank area included multibeam, magnetics, and gravity surveys, as well as rock sampling using seabed rock coring, a remotely operated vehicle (ROV), submersible dives, and dredging (Dick et al., 1991b; MacLeod et al., 1998; Arai et al., 2000; Kinoshita et al., 1999; Matsumoto et al., 2002). A high-resolution bathymetric map of the ~25 km² summit region compiled from narrow-beam echo soundings (Dick et al., 1999) shows the platform consists of a broadly flat surface ranging from ~750 to 689 m water depth (Figure **F5**). ROV survey results show the central pavement to be bare rock, locally knobbly igneous outcrop (largely gabbro) surrounded on its periphery and locally on its surface by limestone, in some places ripple marked, and carbonate-cemented pebble conglomerate. Morphologically the platform is interpreted as a set of partially eroded sea stacks surrounded by beach gravel and limestone pavement (see below).

Figure F5. High-resolution contoured narrow-beam bathymetry map of Atlantis Bank wave-cut platform (Dick et al., 1999), showing ROV and submersible dive tracks plus locations of shallow and deep drill holes (MacLeod et al., 1998).

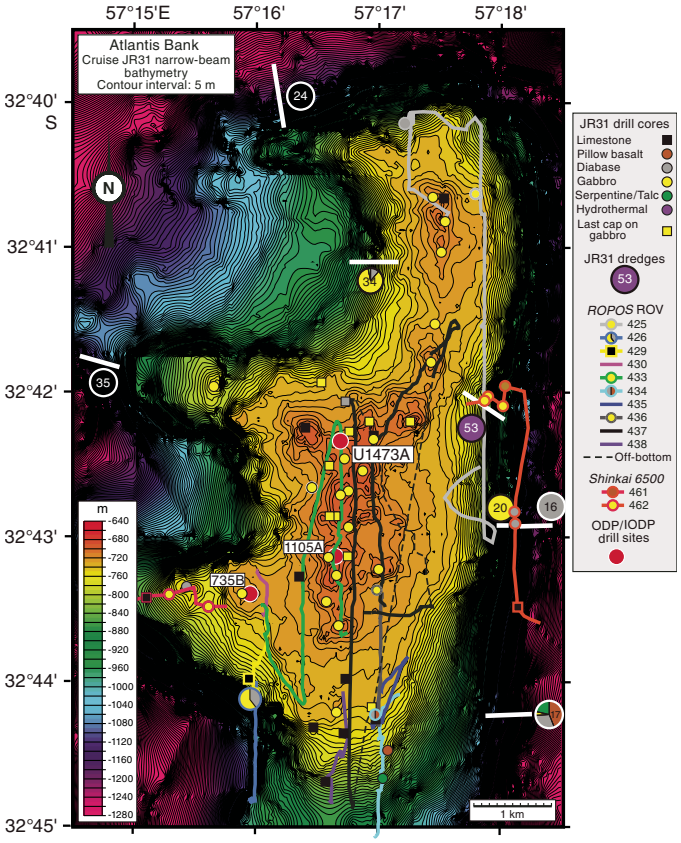

Hole 735B is located at the southwest corner of the relatively flat surface of the Atlantis Bank platform (32°43.395′S, 57°15.959′E, 731 m water depth) (Figures **F3**, **F5**). During Legs 118 and 176, the hole was drilled to a total of 1508 mbsf with 87% core recovery, all in ~11 Ma gabbro (sensu lato) (Robinson, Von Herzen, et al., 1989; Dick et al., 2000). Subsequently, 158 m deep Hole 1105A was drilled during engineering Leg 179 in the center of the platform (32°43.13′S, 57°16.65′E; Pettigrew, Casey, Miller, et al., 1999), also in gabbro and with similar overall core recovery rates.

Employing the British Geological Survey's 5 m diamond rock drill and 1 m "BRIDGE"-oriented corer, RRS *James Clark Ross* Cruise JR31 drilled 42 successful cores on the surface of this platform region, recovering igneous rocks in 33 of them (Figure **F5**) (MacLeod et al., 1998). The cores reveal continuous gabbro outcrop on the platform surface, with diabase at two locations and serpentinized peridotite along with pillow-basalt breccia drilled at its southern tip. The latter two cores were drilled where the flat platform narrows into a north–south spine (32°44.5′S). Many of the gabbroic rocks in the shallow drill cores and seen in *ROPOS* ROV images from the surface of the platform are mylonitic or porphyroclastic, displaying intense crystal-plastic deformation with shallow fabrics. In Hole 735B, crystal-plastic deformation of oxide gabbro and olivine gabbro was likewise found to be strong in the uppermost 500 m but diminished markedly downsection (Robinson, Von Herzen, et al., 1989; Cannat et al., 1991; Dick et al., 1991a; Miranda and John, 2010).

Considered together, it is apparent that the upper surface of Atlantis Bank represents a detachment fault damage zone representing a high-temperature "plutonic growth fault" active during the accretion of the gabbroic lower crust and responsible for its exhumation. This "hot" detachment must have rooted at the top of a continuously replenished crystal mush zone close to the midpoint of the AN-1 spreading ridge (Dick et al., 1991a, 2000; Natland and Dick, 2001, 2002). Numerous inliers of dikes intercalated with gabbro occur across the eastern side of the bank (Figure **F3**), demonstrating that the detachment footwall passed through the zone of active diking beneath the rift valley (Dick et al., 2008). Magnetic anomalies hosted within the gabbro massif indicate it was exposed on a 38.9 km continuously slipping fault over 2.7 My, beginning ~13 Ma and coinciding with accelerated spreading to ~17 mm/y, with sharply increased asymmetry of 14.1 mm/y to the south (Baines et al., 2008). Paleomagnetic remanence inclinations from Holes 735B and 1105A and JR31 seabed drill cores are consistently ~20° steeper than expected for the latitude of Atlantis Bank and are interpreted on the basis of the oriented BRIDGE drill cores as indicating a southward tilt of this magnitude subsequent to cooling of the section through the Curie temperature of magnetite (580°C) (Kikawa and Pariso, 1991; Dick, Natland, Miller, et al., 1999; Pettigrew, Casey, Miller, et al., 1999; Allerton and Tivey, 2001).

Submersible observations at Atlantis Bank (Kinoshita et al., 1999; Matsumoto et al., 2002) show that the detachment fault surface is preserved over large regions in the deeper waters on both sides of the platform. The damage zone and underlying gabbro are well exposed by high-angle normal faulting on the eastern side of the complex and in headwalls of large landslips on the western flank. Here, lower temperature fault rocks are present in addition to the amphibolite facies mylonite. These chloritized and weathered fault gouge and talc-serpentine schists, preserved locally on the fault surface (Dick et al., 2001; Miranda and John, 2010), are very similar to fault rocks found on the Mid-Atlantic Ridge core complexes (e.g., MacLeod et al., 2002; Escartín et al., 2003, Schroeder and John, 2004; Dick et al., 2008).

The absence of the low-temperature fault rocks on the flat surface of the Atlantis Bank platform compared to its flanks suggests they may have been removed, a deduction entirely consistent with the long-held supposition that Atlantis Bank was once an ocean island and that its flat top results from erosion at sea level followed by subsidence to its present level (Dick et al., 1991b; Palmiotto et al., 2013). Shallow drilling and dredging on the summit and uppermost flanks of the Atlantis Bank platform have amply verified this supposition. Indurated carbonates were drilled at 24 sites from the periphery of the platform and were also recovered in dredges from its flanks (MacLeod et al., 1998, 2000; Palmiotto et al., 2013). Although some (recent) carbonate sand was recovered, most of the sediments are indurated bioclastic limestone (skeletal packstone to wackestone; MacLeod et al., 2000) of Miocene to Pleistocene age (Palmiotto et al., 2013). The sediments contain abundant macrofauna, primarily bryozoans, mollusks, algal nodules, and echinoids, but also some solitary corals. Benthic and, in some instances, large planktonic foraminifers are common. Palmiotto et al. (2013) found a water depth of ~100–200 m based on assemblages in dredged carbonates from the flanks of the platform, whereas green algal (dasyclad) assemblages in drill cores from the platform summit (G. Della Porta and V.P. Wright, pers. comm., 1999; MacLeod et al., 2000) indicate water depths at wave base or shallower, demonstrating that the platform was at sea level and probably above. How much material has been removed by subaerial erosion is not known, potentially 100–200 m with reference to the inferred thickness of the detachment fault damage zone. ROV observations of steep-sided outcrops on the platform summit and its flanks up to 10 m, locally even 50 m, likely represent coastal cliffs and small sea stacks resulting from the dispersal of wave energy on the flanks of the island during erosion.

The Atlantis II Transform transverse ridge, on which Atlantis Bank lies, is clearly analogous to oceanic core complex massifs found on the Mid-Atlantic Ridge (e.g., Cann et al., 1997; Tucholke et al., 1998; MacLeod et al., 2002, 2009; Smith et al., 2006; Dick et al., 2008), although here, as elsewhere along the SWIR (Cannat et al., 2006; Sauter et al., 2013), the prominent spreading direction–parallel corrugations that are characteristic of the flat surfaces of the Atlantic oceanic core complexes are not so obvious and are potentially present only on the down-dropped terrace on the eastern side of Atlantis Bank (Figures **F1**, **F3**); furthermore, the Atlantis II Transform transverse ridge was clearly uplifted far above the surrounding seafloor. Whereas flexural uplift of detachment fault footwalls to form oceanic core complexes is typically 1 ± 0.5 km relative to surrounding seafloor of similar age (Tucholke et al., 1998; Lavier et al., 1999), the Atlantis II transverse ridge has been uplifted by 3 km (Baines et al., 2003). Dick et al. (1991a) and Baines et al. (2003) propose that the original detachment-related uplift at the ridge/transform intersection was accentuated by an additional phase of flexural uplift, as transtension was imparted upon the transform in response to a spreading direction change on the SWIR at 19.5 Ma.

One consequence of the Atlantis II transverse ridge relative uplift is that the crust/mantle boundary, as mapped by dredging and submersible traverses, is exposed along its western wall for a distance of nearly 40 km (Figure **F3**). This boundary was encountered at several locations during *Shinkai 6500* dives in landslip headwalls and debris slopes. The boundary lies at ~4660 m water depth west of the drill sites but shoals considerably 20 km to the south, where it was located in outcrop by a *Shinkai 6500* dive at 2563 m water depth (Kinoshita et al., 1999; Matsumoto et al., 2002). Upslope to the east of these dives, Dives 467 and 459 crested the landslip headwalls and encountered the more gently sloping detachment fault footwall at 3000 and 1755 m, respectively, potentially indicating gabbro layer thicknesses as low as 1500 and 2895 m. Elsewhere along the western flank of Atlantis Bank, serpentinized peridotite was recovered in dredges from as shallow as 2000 m water depth (Dredge JR31-DR8), though in other nearby places only at >3000 m depth. At the southern end of the platform summit itself, serpentinized harzburgite was drilled at a water depth of 839 m (Site JR31-BGS12). Highly altered peridotite sampled at several locations above the peridotite/gabbro contact on the transform wall consists largely of talc-serpentine schist that likely overlies the gabbro massif. This and the presence of serpentinized peridotite pebbles in sedimentary (beach) conglomerates lying on gabbro near the edge of the platform suggest that a discontinuous talc-serpentine sheet was intruded along the detachment fault from where the fault cut massive peridotite in the transform fault zone (Dick et al., 2001). This sheet is now preserved locally on the detachment surface. The serpentinite drilled at Site JR31-BGS12 on the southern end of the platform, however, is relatively massive harzburgite with well-preserved pseudomorphs of pyroxene. Possible origins of this particular serpentinite outcrop include a peridotite screen in gabbro similar to those drilled at Atlantis Massif in Integrated Ocean Drilling Program Hole U1309D (Blackman, Ildefonse, John, Ohara, Miller, MacLeod, and the Expedition 304/305 Scientists, 2006), an enclave of less deformed and al-

tered serpentinized peridotite in the original detachment fault shear zone, or juxtaposition via a north-dipping ridge-parallel normal fault that demarcates the southernmost end of the flat platform at 32°44.4′S.

A wide-angle seismic refraction survey of the Atlantis II Transform region found the Moho at 5 ± 1 km beneath Atlantis Bank (Muller et al., 1997, 2000; Minshull et al., 1998) (Figure **F4**). The direct geological constraints outlined above offer strong support to the inference that the Moho cannot represent the (petrological) crust/mantle boundary in this region. Whereas Muller, Minshull, and colleagues also concluded that it could be a serpentinization front, they based this conclusion on the geochemical argument that the igneous crustal thickness there was originally ~4 km (based upon rare earth element inversions), and with the basaltic carapace removed by detachment faulting, the remainder was likely to be ~2 to 2.5 km thick. However, they admit this interpretation is nonunique, primarily because of the overlap in *P*-wave seismic velocity between gabbro and ~20%–40% partially serpentinized peridotite (e.g., Miller and Christensen, 1997).

At what level is the (petrological) crust/mantle boundary likely to lie beneath Atlantis Bank? Projecting the detachment surface to the locations of the traversed crust/mantle boundary described above indicates that the crustal thickness at these points prior to mass wasting on the transform wall was significantly <3 km, whereas the depth to the Moho below the transform wall remains approximately constant (Figure **F4**). Assuming that the elevated core complex massif is produced by flexure during uplift into the rift-mountains because of a spreading direction change (Baines et al., 2003), it seems reasonable to conclude that the mapped boundary is most likely to project approximately subhorizontally or even be elevated beneath the center of Atlantis Bank, consistent with the igneous crustal thickness of 2–2.5 km suggested by Minshull et al. (1998).

Scientific objectives

Previous ODP operations at Atlantis Bank drilled the 1508 m deep Hole 735B and 158 m deep Hole 1105A. Both holes recovered long sections of gabbro, consisting largely of olivine gabbro, subordinate amounts of oxide gabbro, and minor troctolite and leucocratic veins (Dick et al., 1991a, 2000; Pettigrew, Casey, Miller, et al., 1999). On the basis of our previous site survey, we selected Site AtBk6, located on the northern edge of the Atlantis Bank platform 1.4 km north of Hole 1105A and 2.2 km north-northeast of Hole 735B, as the most suitable location for a deep-penetration drill site (Figures **F3**, **F5**).

Three contingency sites identified at Atlantis Bank were Site AtBk4 (serpentinized peridotite Site JR31-BR12) at the southern end of the platform, Site AtBk5 in gabbro at the northern edge of the platform, and Site AtBk2 in gabbro and dikes at 1700 m water depth on the down-dropped terrace east of the main elevated platform (Figures **F3**, **F5**). These sites were envisaged not as alternatives to the deep-penetration site but as single-bit spud-ins in case weather conditions were not sufficiently calm to allow the hard rock reentry system to be deployed at the beginning of the cruise.

Drilling at our principal Site AtBk6 (now Site U1473) during Expedition 360, in lithologies similar to those at previous drill Sites 735 and 1105, was designed to allow us to tackle a number of specific science questions (see below).

1. *What is the igneous stratigraphy of the lower ocean crust?*

   Analysis of drilling results in Hole U1473A should allow us to determine the extent to which the igneous, metamorphic, and structural stratigraphy found in Holes 735B and 1105A is laterally continuous across the wave-cut platform on Atlantis Bank. In combination with Holes 735B and 1105A and the existing surface mapping, new drilling should provide a 3-D and possibly 4-D view of the lateral continuity and evolution of the lower crust and its emplacement process.

2. *How much mantle is incorporated into the lower crust?*

   An unanticipated finding in cores from Hole U1309D at the Atlantis Massif on the Mid-Atlantic Ridge was the incorporation of significant volumes of hybridized mantle peridotite within the gabbro section (Blackman et al., 2011; Expedition 304/305 Scientists, 2006; Drouin et al., 2009). Comparable screens of mantle rock were not found in either Holes 735B or 1105A. Does this reflect a profound difference between the two different mid-ocean ridges, perhaps due to different magma budgets, thermal structure, or accretion mechanisms, or is it simply happenstance that they were not encountered during previous drilling at Atlantis Bank?

3. *What are the modes of melt transport into and through the lower crust?*

   Several different modes of melt delivery and transport were proposed on the basis of observations from Hole 735B cores. These modes include small intrusive cumulate bodies, larger intrusive units on the scale of hundreds of meters, anastomosing channels produced by focused flow and melt-rock reaction, and compaction of late iron titanium–rich melts into shear zones where they hybridized olivine gabbro to iron titanium oxide–rich gabbro and gabbronorite. The continuity and scale of these features cannot be determined from a single deep hole. Results of Expedition 360 drilling should further document the extent and proportion of these features in a younger section of the massif.

4. *How does the lower crust shape the composition of MORB?*

   The complex stratigraphies found in Holes 735B and U1309D differ in significant ways. What common factors, however, influence the composition of MORB? As in Hole 735B, recent work on gabbroic sections from the East Pacific Rise shows that the lower crust acted as a reactive porous filter homogenizing diverse melts that were intruded into it and modifying their trace element contents prior to their eruption to the seafloor (Lissenberg et al., 2013). To what extent does this processes operate uniformly at slower spreading rates?

5. *What is the strain distribution in the lower crust during asymmetric seafloor spreading?*

   Asymmetric spreading produced by detachment faulting is now recognized as one of three major accretionary modes at slow-spreading ridges (symmetric, asymmetric, and amagmatic rifting). Although each of these is important, little is known of how magmatism and tectonism interact, and hence how lower crustal accretion differs in these environments. To date we have been able to determine strain distributions with depth in two deep holes (Holes 735B and U1309D) in two different oceanic core complexes (Atlantis Bank on the SWIR and Atlantis Massif on the Mid-Atlantic Ridge) and found them to differ significantly: far more intense crystal-plastic deformation is found in the upper 500 m of Hole 735B than in Hole U1309D (Figure **F6**). We cannot assess the nature, extent,

Figure F6. Running average (20 m) of lithologies, crystal-plastic deformation intensity, and whole-rock Mg# ([Mg × 100]/[Mg + Fe]) for Holes 735B and U1309D (Mid-Atlantic Ridge at 30°N), modified from Dick et al. (2000), Blackman et al. (2011), and Expedition 304/305 Scientists (2006). Symbols in whole-rock Mg# diagram represent different lithologies based on modal mineralogy; definitions can be found in the Leg 118 and 176 *Initial Reports* volumes (Robinson, Von Herzen, et al., 1989; Dick, Natland, Miller, et al., 1999) and the Expedition 304/305 *Proceedings* volume (Blackman, Ildefonse, John, Ohara, Miller, MacLeod, and the Expedition 304/305 Scientists, 2006). These sections represent descriptions from two different scientific parties, and although both followed American Geophysical Institute conventions on nomenclature, exact definitions for each lithology described may vary. Lithologic plots differ from those previously presented, as the lithologies from both holes were grouped in the same manner to facilitate comparison. Gray dotted lines at Mg# = 80 emphasize overall chemical differences between the sections. Primary melts emerging from the mantle would be in equilibrium with gabbroic cumulates and dunites with an Mg# ≥ 90, largely missing from both sections.

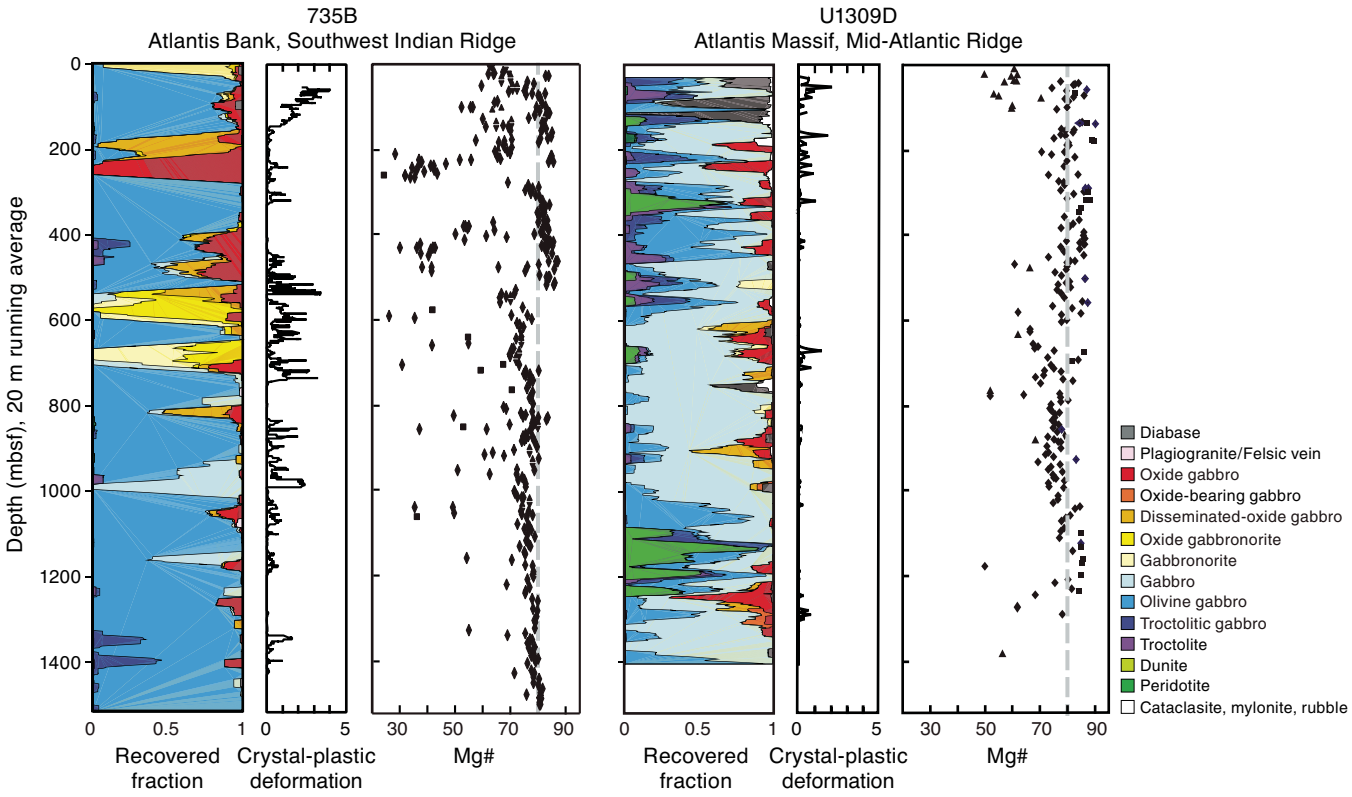

and/or role played by high-temperature deformation during lower crustal accretion with isolated 1-D sections. Offsetting and drilling north of Hole 735B allows determination of the continuity of strain distribution from Holes 735B and 1105A across the Atlantis Bank core complex and thereby assessment of the role and broader significance of synmagmatic deformation in this tectonic environment.

6. What is the nature of magnetic anomalies?

An important goal of Expedition 360 was to drill through a magnetic reversal boundary in oceanic crust for the first time and to determine what controls magnetic anomalies in plutonic rocks.

Magnetic anomaly "stripes" are detectable across the Atlantis II transverse ridge, including Atlantis Bank and its wave-cut platform (Dick et al., 1991b; Allerton and Tivey, 2001; Hosford et al., 2003; Baines et al., 2007, 2008). Whereas most of the platform is reversely magnetized, as are the gabbro intervals of Holes 735B and 1105A (Kikawa and Pariso, 1991), a narrow normal polarity zone ~2 km wide is present near its northern end. This zone is equated to anomaly Chron C5r.2n (11.592–11.647 Ma; Allerton and Tivey, 2001; Baines et al., 2008) (Figure **F7**). The zone is detectable in sea-surface (Dick et al., 1991b; Hosford et al., 2003) and deep-towed magnetic profiles (Allerton and Tivey, 2001), as well as in the JR31 seabed drill cores; however, the precise location of the boundary in each case is slightly offset. Because the sea-surface magnetization signal is derived from a much greater volume of rock than the near-bottom signal in the cores, Allerton and Tivey (2001) deduced from the sense of offset that the magnetic anomaly boundaries are inclined. They modeled the southern limit of the anomaly as a planar boundary dipping ~25° toward the south, suggesting that the surface represented either an isotherm corresponding to the Curie point or the edge of an intrusion. Alternatively, the form of the southern edge of the anomaly may have been modified by faulting: extensive brittle deformation and cataclasis is observed in shallow drill cores from the location of the southern reversal boundary, possibly corresponding to a north-dipping east-west–striking normal fault at the kink/narrowing of the platform summit at 32°41.8′S. If so, the reversal boundary is likely to dip more steeply than the 25° proposed by Allerton and Tivey (2001). For this reason, Hole U1473A was sited at the northern end of the main platform, just south of this normal fault, to encounter the reversal boundary at as a shallow a depth as possible.

7. What is the role of the lower crust and shallow mantle in the global carbon cycle?

Under certain conditions, serpentinization and weathering of ultramafic rocks as well as alteration of basalts are known to cause

Figure F7. A. Location and magnetization of Atlantis Bank platform drill cores. B. Contoured deep-towed magnetization. C. Magnetic anomaly models with positions of Holes 735B and U1473A.

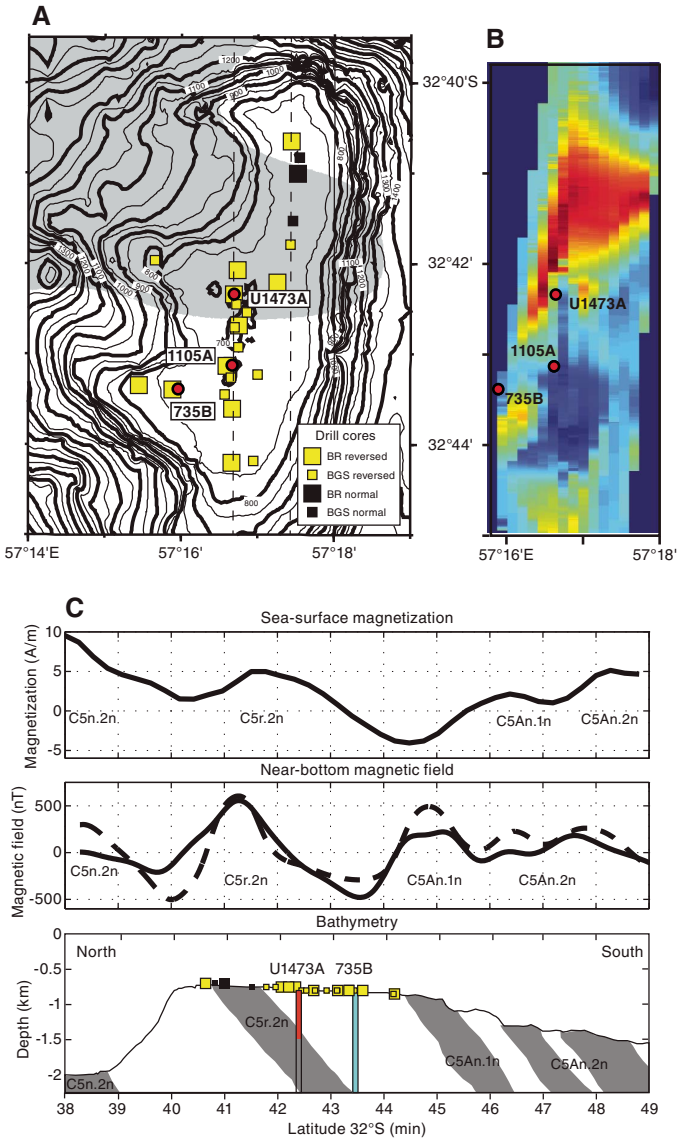

the formation of carbonates. Such carbonates are present in the form of extensive veining in serpentinized peridotite at the southern edge of the Atlantis Bank platform (shallow drill Site JR31-BGS12/contingency drill Site AtBk4) and in partially serpentinized and weathered peridotite from the southern transform wall at 32°50′S (*Kaiko* ROV Dives 173 and 174).

The extent of these reactions in the lower crust is largely unknown to date. We do not expect that carbon sequestration will be a significant process in the lower ocean crust based on Holes 735B and U1309D; however, the possibility exists that Expedition 360 may penetrate the base of the lower ocean crust, and thus offer the first opportunity to determine if carbon sequestration is significant in the mantle below it.

8. Is there life in the lower crust and hydrated mantle?

A primary objective of the SloMo Project is to determine the microbiology of the lower crust, the potential serpentinized mantle above the Moho, and the underlying mantle to address IODP Science Plan Challenge 6 "What are the limits of life in the subseafloor?"

Starting in the 1990s, microbiologists accompanying ODP and Integrated Ocean Drilling Program expeditions have documented the presence of microbial life in deeply buried sediment and the basaltic basement (Fisk et al., 1998; Parkes et al., 1994; Mason et al., 2010). Evidence for active microbial life has been detected as deep as 2458 mbsf (Inagaki et al., 2015), and the introduction of molecular biology into marine ecology has led to great advances in our understanding of microbial life below the seafloor (Biddle et al., 2008; Cowen et al., 2003; Inagaki et al., 2006; Mason et al., 2010; Edgcomb et al., 2011; Orsi et al., 2013a, 2013b). Much of the microbiology performed during ODP and Integrated Ocean Drilling Program expeditions has concentrated on sediment (e.g., ODP Leg 201 to the Peru margin), with the notable exception of expeditions to the Juan de Fuca Ridge (Cowen et al., 2003; Lever et al., 2013; Jungbluth et al., 2013), Atlantis Massif (Mason et al., 2010), North Pond (Orcutt et al., 2013), and Louisville Seamounts (Sylvan et al., 2015).

Because it was never expected that mantle rocks would be encountered during the first phase of SloMo, the aim of microbiology sampling during Expedition 360 was to explore for evidence of microbial life at depth within the crystalline lower oceanic crust, about which little is known. It is nevertheless possible that indirect inferences may be drawn as to the likely processes at work at greater depths from a microbial perspective based on postcruise analysis of gabbros drilled during the expedition. Olivine-rich gabbros can host serpentinization, a process that produces hydrogen, which can serve as an electron donor for microbial metabolism. Serpentinization can also be an abiotic methanogenic process through Fischer Tropsch type reactions (CO_2 reduction with H_2 in aqueous solution; Proskurowski et al., 2008), thus potentially providing an additional source of carbon (in addition to carbon dioxide that may be present) for life in the deep crust. Complex organic matter and lipids in serpentinites suggest microorganisms inhabit mantle rock exhumed at the seafloor (Delacour et al., 2008; Ménez et al., 2012). In cores from Hole U1309D (Atlantis Massif), small subunit ribosomal RNA gene sequence analyses indicated that heterotrophic microorganisms putatively capable of hydrocarbon oxidation are present in lower crustal rocks (Mason et al., 2010). Delacour et al. (2008) point out that organics in these systems likely have both biotic and abiotic sources. Abiotic synthesis of organics during serpentinization is a way of providing energy to deep-seated communities, but inorganic redox fluid-mineral reactions may also be mined directly for metabolic energy (e.g., Shock, 2009). Apart from energy constraints, permeability and the distribution of fluid flow impose strong constraints on the presence and activity of subseafloor life, and these factors can only be accurately determined by drilling. During Expedition 360, microbiologists focused on exploring evidence of life using culture-based approaches, molecular analyses, microscopy, and enzyme assays. Efforts were focused on rock sections showing evidence of alteration or fracturing within all lithologies encountered.

Site survey

The broad location of the deep-penetration SloMo legacy hole that was envisaged to be drilled during Expedition 360 was the north central part of Atlantis Bank, south of the inferred north-dipping fault that coincides with the bathymetric offset of the platform at 32°42′S. We believed this location would be away from the influ-

ence of the fault zone yet close to the inferred south-dipping magnetic reversal boundary, and it would be sufficiently distant from Holes 735B and 1105A to allow us to assess kilometer-scale variability of magmatic and tectonic processes associated with lower crustal accretion.

The site selected for deep drilling (proposed Site AtBk6) was cored during the 1998 site survey Cruise JR31 as Site JR31-BR8, determined to be located at 32°42.3402′S, 57°16.6910′E, on the basis of an acoustic transponder network deployed during Cruise JR31 on the *James Clark Ross* (MacLeod et al., 1998). From a seafloor photograph taken from the BRIDGE drill camera the site was deemed to be part of an extensive bare-rock pavement outcrop (Figure **F8**). Drill Core JR31-BR8 consisted of 1.1 m of oxide-bearing olivine gabbronorite with a thin mylonitic shear zone.

Following the transit from Sri Lanka, we headed directly for Site AtBk6. Once on site, an advanced piston corer (APC)/extended core barrel (XCB) bit, bit sub, drill collars, and 5 inch drill pipe assembly was assembled and lowered to 668 meters below rig floor (mbrf). The subsea camera system was installed and lowered to just above the bit to conduct a survey to select a site appropriate for drilling. The survey strategy was to proceed in a square "spiral" pattern increasing at 10 m intervals away from the Site AtBk6 start point until a sufficiently flat bare-rock spot at least 5 m in diameter was located. The drill pipe and camera were raised and lowered by up to several meters as required by the seafloor morphology.

No suitable site was found at Site AtBk6 or during the initial 50 m × 50 m survey (Figure **F9**); rather than the bare-rock pavement photographed at Site JR31-BR8, we observed white sediment plus scattered dark (gabbro) blocks on a near-flat surface deepening slightly to the northwest (Figures **F9**, **F10A–F10B**). The reason for the disparity with what was previously observed at apparently the exact same location is not known but probably indicates some absolute offset of some tens of meters in the navigation of the JR31 transponder survey.

The initial 50 m × 50 m survey spiral revealed a dense boulder field and possible outcrop at the southwestern corner of the box; accordingly, the survey was extended south and southwest by a further 50 m. Within this area, an irregular steep-sided outcrop of dark gabbro was identified, north-northwest elongated, ~30 m wide by >60 m long, and rising abruptly by as much as ~10 m above the surrounding carbonate sediment-covered seafloor. The top of this outcrop was flat and formed either of bare gabbro exposures or by a thin cap of indurated carbonate. After further investigation of the flat bare-rock pavement after 5.5 h of survey, a suitable location for Hole U1473A was found (Figure **F10E–F10F**) at 32°42.3622′S, 057°16.6880′E (710.2 mbsl), 40 m south of the original start point.

Figure F8. Target area selected for deep drill site (proposed Site AtBk6), showing flat bare-rock pavement (with echinoid) and thin carbonate in distance. Leg of BRIDGE seabed rock drill is in the foreground; drilling here (Site JR31-BR8) yielded 1.1 m of oxide-bearing olivine gabbronorite cut by a thin mylonitic shear zone. Field of view = ~4–5 m.

Figure F9. Track map of subsea camera system during Site AtBk6/U1473 survey. The initial 50 m × 50 m box was extended south and west when it was clear that the seafloor at and around the original Site AtBk6 location (Waypoint 1) was dominated by sediment and scattered blocks of gabbro. Local bathymetry was derived from pipe length measurements combined with estimate of distance of pipe off the bottom for each minute of the survey.

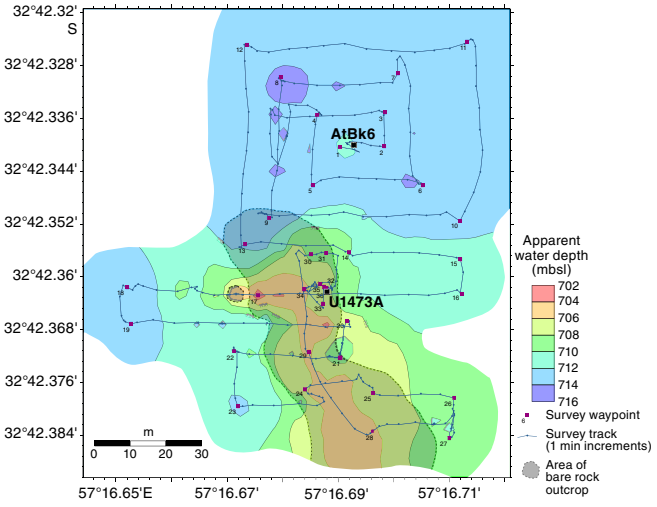

Figure F10. A–E. Various stages (waypoints) of site survey (locations shown in Figure F9). Dark lineaments in D are believed to be east-west–trending amphibole veins. E. Site chosen for Site U1473. F. Hole U1473A hard rock reentry system in place on seafloor. Drill pipe is 9⅞ inches in diameter (~25 cm).

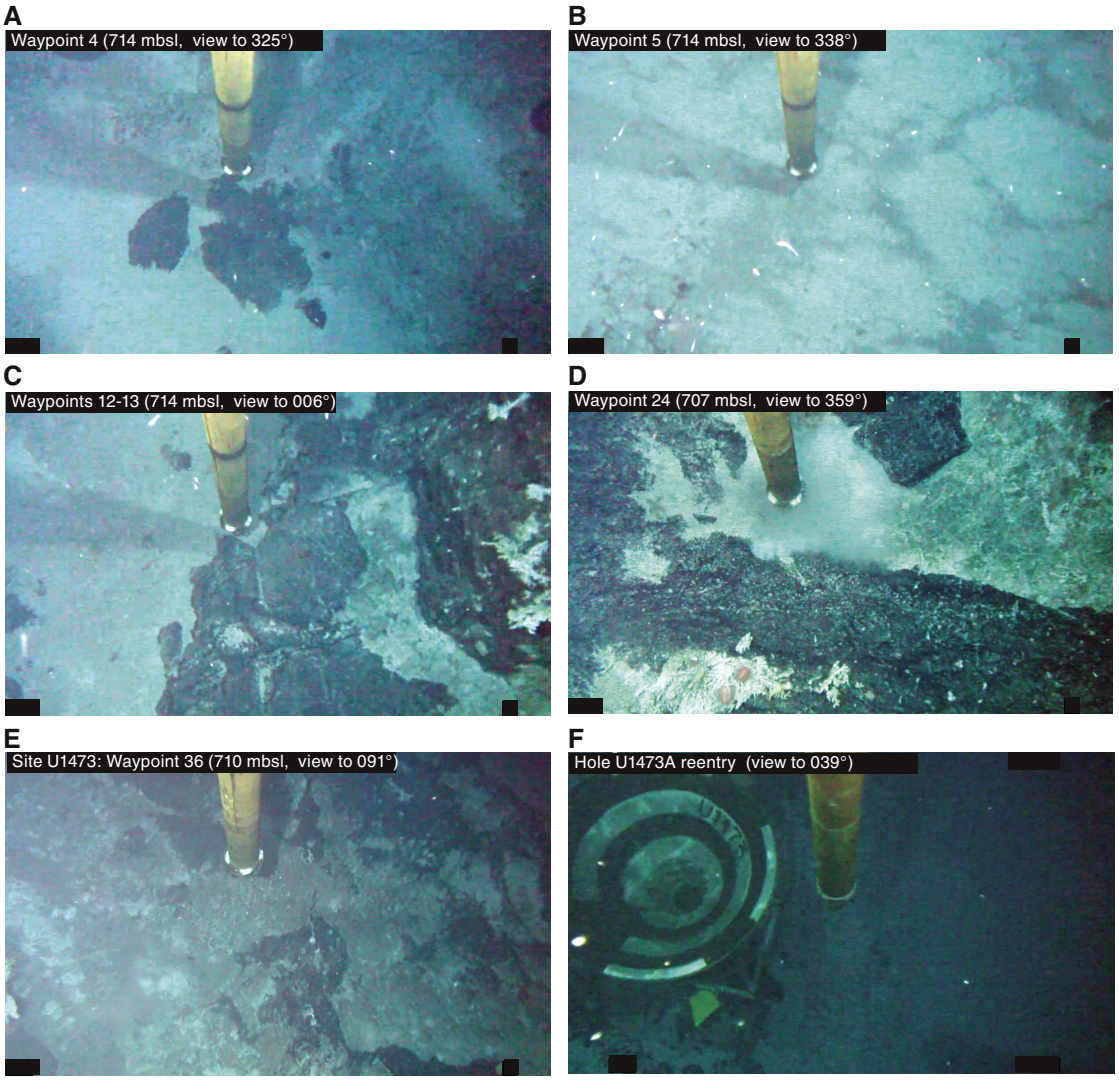

Principal results

Site U1473

Hole U1473A is located at 32°42.3622′S 57°16.6880′E, in 710.2 m water depth on the north central part of Atlantis Bank, 2.2 km north-northeast of Hole 735B and 1.4 km north of Hole 1105A. During Expedition 360, Hole U1473A was drilled to a total depth of 789.7 m DSF, recovering 469.4 m of core with an average of 59% recovery over the entire interval (>96% over the lower 200 m of the hole; Table T1). This constitutes the deepest igneous rock penetration from the seafloor during a single scientific ocean drilling expedition to date.

Igneous petrology

Hole U1473A cores are composed of a variety of gabbroic lithologies, from primitive olivine gabbros to evolved oxide-rich gabbros, cut by felsic veins (~1.5% of the total), as well as a small number of diabase dikes. Eight lithologic units were defined within the gabbroic sequence, primarily on the basis of changes in mineral modes, grain size, and texture but also based on the presence and relative importance of other igneous features such as igneous layering and felsic material (Figure F11). Magnetic susceptibility and bulk-rock geochemical variations were also considered when defining these units.

Primary magmatic textures of gabbros to ~400 m core composite depth below seafloor (CCSF) are heavily modified or in many cases erased by intense crystal-plastic deformation; when preserved, primary textures are mostly subophitic and locally granular. The main lithology is olivine gabbro (76.5%), followed in abundance by disseminated-oxide gabbro (9.5%; oxide content between 1% and 2%), gabbro (sensu stricto; 5.1%), oxide gabbro (3.7%; oxide content >5%), oxide-bearing gabbro (3.7%; oxide content between 2% and 5%), and felsic veins (1.5%). Oxide abundance decreases slightly downhole, with the exception of the lowermost intervals (deeper than ~650 m CCSF) within which a larger proportion of oxide-bearing lithologies was recovered. Oxide-bearing gabbro and oxide gabbro are usually characterized by strong localized crystal-plastic deformation; however, in contrast, those in the deepest part of Hole U1473A (Unit VIII) are essentially undeformed. Formation of oxide gabbro is most likely related to the percolation of late-stage melts through an existing olivine gabbro framework, an inference that is supported by the near-ubiquitous presence of interstitial brown am-

Table T1. Site U1473A core summary. For more information on bottom-hole assembly (BHA) runs, see Table **T2** in the Site U1473A chapter (MacLeod et al., 2017b). DRF = drilling depth below rig floor, DSF = drilling depth below seafloor, CSF-A = core depth below seafloor, method A. Core type: G = ghost, M = miscellaneous, R = rotary core barrel (RCB), numeric core type = drilled interval. MBR = mechanical bit release. (Continued on next page.) **Download table in .csv format.**

Hole U1473A
Latitude: 32°42.3622′S
Longitude: 057°16.6880′E
Water depth (m): 710.23
Date started (UTC): 1300 h; 16 December 2015
Date finished (UTC): 0430 h; 27 January 2016
Time on hole (days): 41.65
Seafloor depth DRF (m): 721
Rig floor to sea level (m): 10.77
Penetration DSF (m): 789.7
Cored interval (m): 742.7
Recovered length (m): 469.15
Recovery (%): 63
Drilled interval (m): 47
Drilled interval (no.): 2
Total cores (no.): 89
RCB cores (no.): 86
Other cores (no.): 3

Core	Top depth drilled DSF (m)	Bottom depth drilled DSF (m)	Interval advanced (m)	Recovered length (m)	Curated length (m)	Core recovery (%)	Top depth cored CSF-A (m)	Bottom depth recovered CSF-A (m)	Core on deck date	Core on deck time UTC (h)	Sections (*N*)	BHA run number	Operational episode description
360-U1473A-													
11			****Drilled interval from 0.00 to 9.5 m DSF*****						18 Dec 2015	1445	0	2	Install reentry system
2R	9.5	12.8	3.3	2.25	2.45	68	9.5	11.95	19 Dec 2015	2345	2	3	Coring Episode 1
3R	12.8	22.4	9.6	4.24	5.10	44	12.8	17.90	20 Dec 2015	0535	4		
4R	22.4	32.0	9.6	6.27	8.41	65	22.4	30.81	20 Dec 2015	1230	6		
5R	32.0	41.6	9.6	2.07	2.05	22	32.0	34.05	20 Dec 2015	1615	2		
6R	41.6	51.3	9.7	3.08	4.08	32	41.6	45.68	20 Dec 2015	1950	3		
7R	51.3	61.0	9.7	1.92	2.27	20	51.3	53.57	21 Dec 2015	0005	2		
8R	61.0	70.7	9.7	4.92	5.82	51	61.0	66.82	21 Dec 2015	0610	4		
9R	70.7	80.4	9.7	5.92	7.14	61	70.7	77.84	21 Dec 2015	1045	5		
10R	80.4	90.1	9.7	3.07	3.43	32	80.4	83.83	22 Dec 2015	0355	3	4	
11R	90.1	99.8	9.7	6.19	7.01	64	90.1	97.11	22 Dec 2015	0820	5		
12R	99.8	109.5	9.7	6.30	6.68	65	99.8	106.48	22 Dec 2015	1135	5		
13R	109.5	119.2	9.7	5.42	5.85	56	109.5	115.35	22 Dec 2015	1625	5		
14R	119.2	128.9	9.7	6.09	7.16	63	119.2	126.36	22 Dec 2015	2225	5		
15R	128.9	138.6	9.7	7.21	8.70	74	128.9	137.60	23 Dec 2015	0340	7		
16R	138.6	148.3	9.7	7.84	8.83	81	138.6	147.43	23 Dec 2015	1010	6		
17R	148.3	158.0	9.7	5.94	7.06	61	148.3	155.36	23 Dec 2015	1550	5		
18R	158.0	167.7	9.7	4.64	5.48	48	158.0	163.48	23 Dec 2015	2350	4		
19R	167.7	177.4	9.7	2.30	3.01	24	167.7	170.71	24 Dec 2015	1305	2	5	
20R	177.4	180.1	2.7	2.15	2.44	80	177.4	179.84	24 Dec 2015	1530	2		
21R	180.1	187.1	7.0	4.00	4.60	57	180.1	184.70	25 Dec 2015	1225	4		
22R	187.1	196.8	9.7	1.56	1.95	16	187.1	189.05	25 Dec 2015	1510	2		
23R	196.8	206.5	9.7	4.12	5.69	42	196.8	202.49	25 Dec 2015	1815	4		
24R	206.5	216.2	9.7	3.67	4.83	38	206.5	211.33	25 Dec 2015	2135	4		
25R	216.2	225.9	9.7	2.65	3.33	27	216.2	219.53	26 Dec 2015	0130	3		
26R	225.9	235.6	9.7	3.28	4.24	34	225.9	230.14	26 Dec 2015	0615	3		
27R	235.6	245.3	9.7	7.48	8.23	77	235.6	243.83	26 Dec 2015	1000	6		
28R	245.3	255.0	9.7	7.22	7.35	74	245.3	252.65	26 Dec 2015	1400	5		
29R	255.0	264.7	9.7	6.82	7.34	70	255.0	262.34	26 Dec 2015	1820	5		
30R	264.7	274.4	9.7	5.79	6.64	60	264.7	271.34	26 Dec 2015	2135	5		
31R	274.4	284.1	9.7	2.70	3.65	28	274.4	278.05	27 Dec 2015	0010	3		
32R	284.1	293.8	9.7	7.43	8.72	77	284.1	292.82	27 Dec 2015	0400	6		
33R	293.8	303.5	9.7	6.03	6.65	62	293.8	300.45	27 Dec 2015	0810	5		
34R	303.5	313.2	9.7	6.77	7.53	70	303.5	311.03	27 Dec 2015	1210	6		
35R	313.2	322.9	9.7	2.40	2.89	25	313.2	316.09	28 Dec 2015	0220	2	6	
36R	322.9	332.6	9.7	3.02	3.92	31	322.9	326.82	28 Dec 2015	0530	3		
37R	332.6	342.3	9.7	4.57	5.90	47	332.6	338.50	28 Dec 2015	0855	4		
38R	342.3	352.0	9.7	4.36	5.06	45	342.3	347.36	28 Dec 2015	1415	4		
39R	352.0	361.7	9.7	7.06	8.37	73	352.0	360.37	28 Dec 2015	1850	6		
40R	361.7	371.4	9.7	2.17	2.41	22	361.7	364.11	29 Dec 2015	0040	2		
41R	371.4	381.1	9.7	7.09	7.99	73	371.4	379.39	29 Dec 2015	0520	6		
42R	381.1	390.8	9.7	4.06	4.92	42	381.1	386.02	29 Dec 2015	0935	4		
43R	390.8	400.5	9.7	9.25	10.02	95	390.8	400.82	29 Dec 2015	1440	8		

Table T1 (continued).

Core	Top depth drilled DSF (m)	Bottom depth drilled DSF (m)	Interval advanced (m)	Recovered length (m)	Curated length (m)	Core recovery (%)	Top depth cored CSF-A (m)	Bottom depth recovered CSF-A (m)	Core on deck date	Core on deck time UTC (h)	Sections (*N*)	BHA run number	Operational episode description
44R	400.5	410.2	9.7	5.44	6.42	56	400.5	406.92	29 Dec 2015	2140	5		
45M	410.2	410.8	0.6	0.50	1.25	83	410.2	411.45	7 Jan 2016	1130	1	10	Fishing for roller cones
46R	410.8	420.5	9.7	2.59	3.94	27	410.8	414.74	8 Jan 2016	0425	3	11	Coring Episode 2 and two roller cones lost and found
47R	420.5	430.2	9.7	4.04	5.29	42	420.5	425.79	8 Jan 2016	0815	4		
48R	430.2	439.9	9.7	2.69	3.83	28	430.2	434.03	8 Jan 2016	1035	3		
49R	439.9	449.6	9.7	0.98	1.31	10	439.9	441.21	8 Jan 2016	1830	1		
50R	449.6	459.3	9.7	3.52	4.50	36	449.6	454.10	9 Jan 2016	0015	3		
51R	459.3	469.0	9.7	5.72	6.40	59	459.3	465.70	9 Jan 2016	0505	5		
52R	469.0	469.6	0.6	0.42	0.49	70	469.0	469.49	9 Jan 2016	0725	1		
53R	469.6	470.6	1.0	0.00	0.00	0	469.6	469.60	11 Jan 2016	0045	0	14	Advance limited; recovery prevented by roller cone stuck in bit
54R	470.6	480.3	9.7	0.00	0.00	0	470.6	470.60	11 Jan 2016	0635	0		
55R	480.3	481.7	1.4	0.00	0.00	0	480.3	480.30	11 Jan 2016	1100	0		
561		*****Drilled interval from 481.7 to 519.2 m DSF*****							13 Jan 2016	1130	0	16	Drilling without coring
57R	519.2	519.6	0.4	0.40	0.40	100	519.2	519.60	14 Jan 2016	0400	1	17	Coring Episode 3
58R	519.6	529.2	9.6	9.48	10.35	99	519.6	529.95	14 Jan 2016	0750	8		
59R	529.2	538.8	9.6	6.50	6.84	68	529.2	536.04	14 Jan 2016	1315	5		
60R	538.8	548.4	9.6	5.16	6.19	54	538.8	544.99	14 Jan 2016	1845	5		
61R	548.4	558.1	9.7	6.72	7.61	69	548.4	556.01	15 Jan 2016	0040	6		
62R	558.1	567.8	9.7	7.01	7.63	72	558.1	565.73	15 Jan 2016	0420	6		
63R	567.8	577.5	9.7	2.22	2.72	23	567.8	570.52	15 Jan 2016	0830	2		
64R	577.5	587.2	9.7	9.37	9.76	97	577.5	587.26	15 Jan 2016	1350	9		
65R	587.2	596.9	9.7	9.32	9.77	96	587.2	596.97	15 Jan 2016	2045	7		
66R	596.9	606.6	9.7	8.74	9.06	90	596.9	605.96	16 Jan 2016	0235	7		
67R	606.6	616.3	9.7	9.73	10.32	100	606.6	616.92	16 Jan 2016	2125	8	18	
68R	616.3	626.0	9.7	9.23	9.67	95	616.3	625.97	17 Jan 2016	0235	7		
69R	626.0	635.7	9.7	9.80	10.26	101	626.0	636.26	17 Jan 2016	0850	8		
70R	635.7	645.4	9.7	8.87	9.09	91	635.7	644.79	17 Jan 2016	1415	8		
71R	645.4	648.4	3.0	3.62	3.76	121	645.4	649.16	17 Jan 2016	1805	3		
72R	648.4	651.9	3.5	3.60	3.71	103	648.4	652.11	18 Jan 2016	1145	3	19	
73R	651.9	654.6	2.7	1.85	2.03	69	651.9	653.93	19 Jan 2016	0050	2	20	
74R	654.6	664.3	9.7	10.09	10.35	104	654.6	664.95	19 Jan 2016	0605	9		
75R	664.3	674.0	9.7	9.88	10.28	102	664.3	674.58	19 Jan 2016	1120	8		
76R	674.0	680.7	6.7	5.16	5.31	77	674.0	679.31	19 Jan 2016	1710	5		
77R	680.7	683.7	3.0	2.29	2.42	76	680.7	683.12	19 Jan 2016	2115	2		
78R	683.7	693.4	9.7	9.94	10.56	102	683.7	694.26	20 Jan 2016	0330	8		
79R	693.4	703.1	9.7	8.94	9.54	92	693.4	702.94	20 Jan 2016	0805	8		
80R	703.1	712.8	9.7	9.86	10.26	102	703.1	713.36	20 Jan 2016	1440	9		
81R	712.8	721.3	8.5	7.62	8.55	90	712.8	721.35	20 Jan 2016	2155	6		
82R	721.3	731.0	9.7	9.80	10.01	101	721.3	731.31	21 Jan 2016	1745	8	21	
83R	731.0	740.7	9.7	9.64	10.00	99	731.0	741.00	22 Jan 2016	0205	9		
84R	740.7	750.4	9.7	9.52	9.75	98	740.7	750.45	22 Jan 2016	0705	7		
85R	750.4	756.1	5.7	5.04	5.27	88	750.4	755.67	22 Jan 2016	1325	4		
86R	756.1	760.1	4.0	3.27	3.38	82	756.1	759.48	22 Jan 2016	1720	3		
87R	760.1	769.8	9.7	9.64	9.88	99	760.1	769.98	22 Jan 2016	2340	9		
88R	769.8	779.5	9.7	9.39	9.72	97	769.8	779.52	23 Jan 2016	0445	8		
89R	779.5	789.2	9.7	9.73	10.06	100	779.5	789.56	23 Jan 2016	1000	8		
90G	9.5	789.2	779.7	0.25	0.25		9.5	9.75	25 Jan 2016	1500	1	22	Successful logging (MBR problem)
91M	789.2	789.7	0.5	0.50	0.50	100	789.2	789.70	27 Jan 2016	0230	1	24	
		Total:	1569.4	469.4									

phibole and rims around clinopyroxene and/or olivine. When located around olivine, brown amphibole is also associated with orthopyroxene rims. These late-stage melt-related features are less abundant in undeformed samples from the deeper levels of the hole. Felsic veins consist of leucodiorite, quartz diorite, diorite, trondhjemite, and rare tonalite, locally containing oxide minerals. They tend to be concentrated in specific zones or horizons, with trondhjemite predominating deeper than 500 m CCSF.

Several dikelike bodies of diabase were found at various depths in Hole U1473A. They intrude gabbros that had experienced previous crystal-plastic deformation under conditions ranging from granulite down to amphibolite facies. Most of the dikes have diabasic textures; however, the larger granulite facies dikes have local assemblages of granoblastic brown amphibole, plagioclase, clinopyroxene, and orthopyroxene near their contacts with the gabbro, reflecting recrystallization, likely at 800°C or higher. Likely associated centimeter-scale dikelets may consist entirely of the granulite assemblage. From textural relationships, some dikes appear to have locally partially melted the adjacent gabbro to form the felsic veins.

Figure F11. Lithostratigraphic variations, Hole U1473A. Relative abundances of rocks are averaged over 20 m. Dashed lines = unit boundaries. Histograms document proportion of felsic veins per section and number of igneous layers identified every 5 m. Length of vein/10 m core is calculated as total sum of vein length (in centimeters) every 10 m of core.

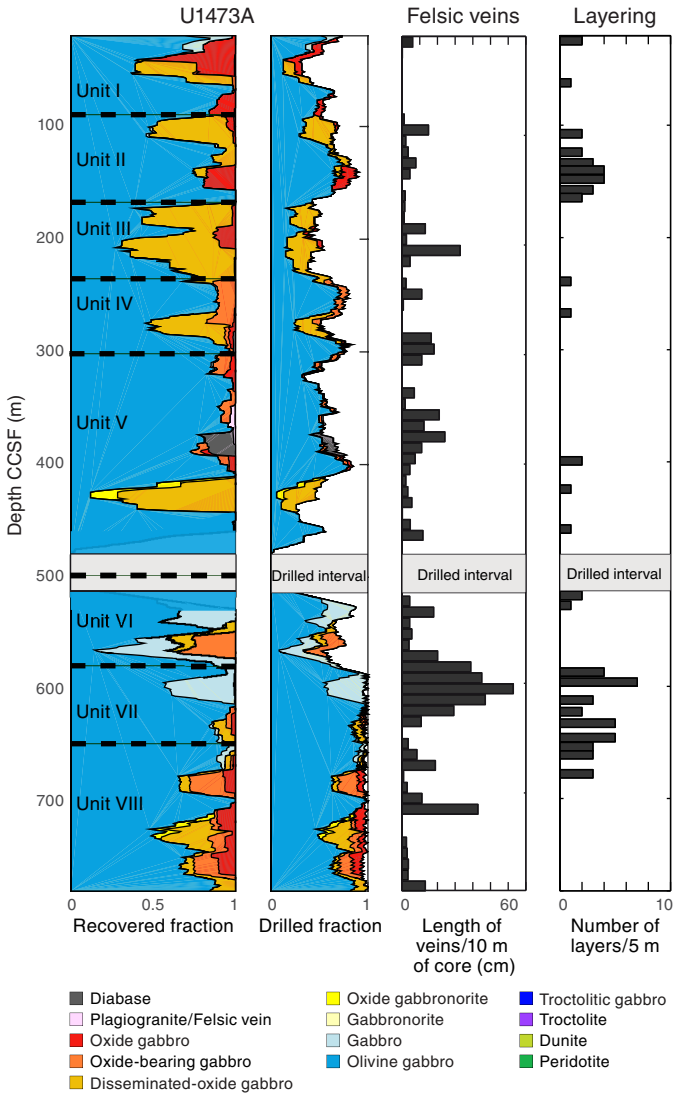

Igneous layering, defined by modal and grain size variation, is well developed in Units II and VII (91.29–175 and 577.68–642 m CCSF, respectively). Grain size variability in the layering is generally also accompanied by modal variation. In most cases, contacts between different layers are subparallel to each other, though less commonly irregular contacts are also found. The dominant olivine gabbro is largely coarse grained but locally displays considerable variability, ranging from fine to very coarse grained. Grain size variations in olivine gabbro may be locally associated with igneous layering but are mainly found within irregular olivine gabbro domains with sutured contacts. The degree to which the igneous layering here and in Holes 735B and 1105A can be interpreted in terms of magmatic sedimentation as seen in layered intrusions is problematic and often appears to be the product of processes such as late-stage melt-rock interaction, focused melt flow through a crystal mush, or melts migrating along zones of deformation.

In several respects Hole U1473A displays close similarities to the other two holes drilled at Atlantis Bank (Holes 735B and 1105A; Dick et al., 2000; Casey et al., 2007) (Figure **F12**). Similar igneous processes operated in the genesis of the plutonic section as a whole. Most striking is the first-order observation that the plutonic sections in Holes 735B and U1473A are mainly composed of olivine gabbro (>75%) with numerous intercalations of gabbros containing oxides (~15% of the sections). The level and volume of oxide and disseminated-oxide gabbros vary considerably between the Atlantis Bank drill sites. It is probable that more of the section was removed by erosion at Site U1473 compared to Site 735, making direct correlation of the sections relative to the detachment fault surface difficult. Intensely deformed and/or oxide-rich intervals are abundant in the upper portion of Hole 735B and decrease rapidly deeper than 600 mbsf; they are abundant in 158 m deep Hole 1105A, and although present in Hole U1473A, they occur intermittently downhole with a larger abundance of the related disseminated-oxide gabbro.

Felsic rocks are also found ubiquitously across Atlantis Bank (e.g., Baines et al., 2008) and at all three drill sites. These rocks are represented by veins or patches that are reported to be associated with oxide gabbros in Hole 735B (Dick et al., 2000) and with olivine gabbro in Hole 1105A (Casey et al., 2007) but are found associated with or cutting both rock types in Hole U1473A. Locally, some dike margins are invaded by felsic melts that were most likely generated by contact metamorphism of the previously hydrothermally altered host gabbro. Other felsic veins may be the product of extreme fractionation of the gabbroic melts or even local anatexis of gabbros due to subsequent gabbro intrusive cycles (e.g., Koepke et al., 2004).

Troctolite and troctolitic gabbro found in Hole 735B and, in the first case, interpreted as representing injection of primitive melts into the crystallizing olivine gabbros, were not encountered in Hole U1473A.

Another common feature of the three holes drilled at Atlantis Bank is the occurrence of 100–400 m thick igneous lithologic units defined by variations in texture, grain size, mode, and geochemical composition. These units are mirrored by variations in whole-rock geochemical compositions, which reveal apparent upward-differentiating geochemical trends, as defined by decreases in Mg# and Cr and Ni contents and increases in Y (Figure **F13**) (see **Geochemistry** below). Each of the lithologic units is in turn characterized by internal heterogeneity in composition and texture on a meter or even centimeter scale, seen in Hole 735B and U1473A cores. This heterogeneity was likely governed by complex interplay between magmatic processes, such as new melt injections, fractional crystallization, melt-rock reaction, and late-stage melt migration with deformation. It is not clear, however, whether these units represent progressive fractional crystallization of a melt or simply compaction of late interstitial melts moving up through the section.

Taken as a whole, the igneous stratigraphies of Holes 735B, 1105A, and U1473A document directly comparable processes that occurred at all three locations over a lateral scale of >2 km and vertical scale of ≥1.5 km. This leads us to suggest that this portion of the Atlantis Bank plutonic section is relatively homogeneous laterally. Key features are (i) the occurrence of olivine gabbro as the principal lithology; (ii) the ubiquitous presence of disseminated-oxide, oxide-bearing, and oxide gabbros and their greater abundance at the shallower structural levels; and (iii) the presence of ~100–400 m thick olivine gabbro units showing upward-differentiated geochemical trends that may represent discrete magma bodies. Whereas the different drill holes display striking similarities between each other overall, we do not attempt to correlate specific igneous units directly from hole to hole; instead, we prefer to emphasize the similarity in overall igneous accretion processes and gross stratigraphy.

Figure F12. Hole U1473A lithostratigraphic variations compared with lithostratigraphic columns for other holes drilled at Atlantis Bank (Holes 735B and 1105A) and Atlantis Massif (Hole U1309D). Relative abundances of rocks are averaged over 20 m. In Holes 735B and U1309D, oxide gabbro includes both oxide gabbro and oxide-bearing gabbro. Gray bar = drilled interval.

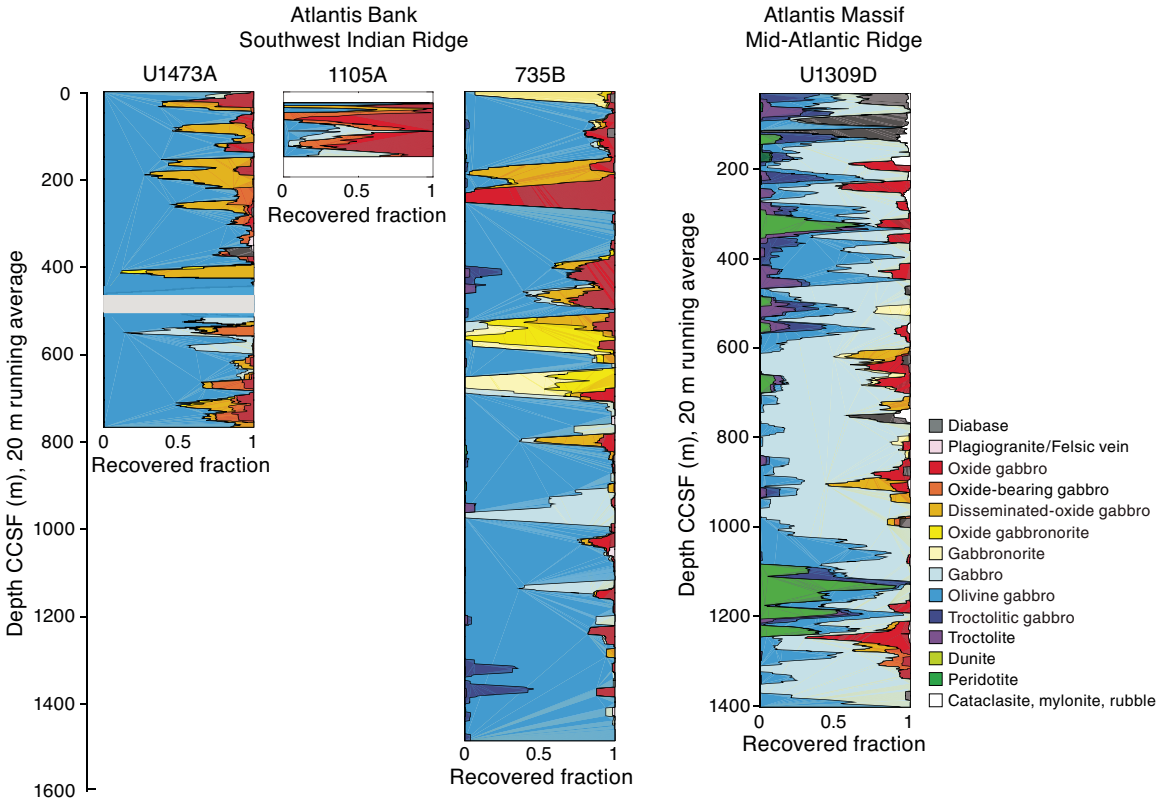

Figure F13. Chemical variations as a function of depth, Hole U1473A. Mg# decreases over most of the hole with discontinuities at ~60, ~300, and 700 m CCSF (dotted lines). Ni and Cr data define geochemical boundaries with abrupt changes in concentration at ~60, 300, and 700 m CCSF. Olivine gabbros collected to investigate alteration are distinguished.

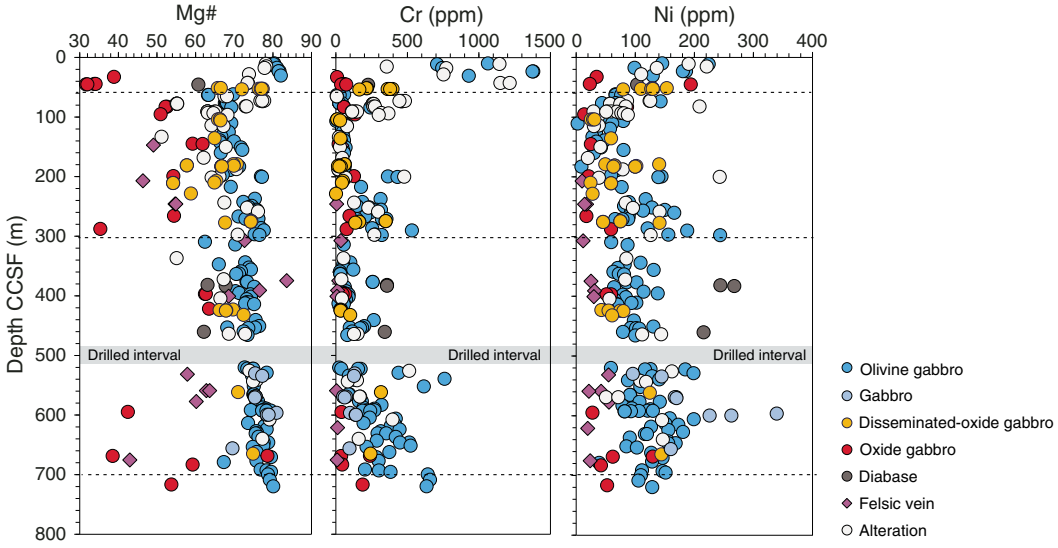

How applicable are the conclusions we draw from drilling at Atlantis Bank to other oceanic core complex gabbro massifs or, indeed, plutonic accretion processes at (slow-spreading) mid-ocean ridges in general? In partial answer to this question, we compare the igneous architecture documented at Atlantis Bank with that of the gabbro body drilled at Atlantis Massif, the oceanic core complex at 30°N on the Mid-Atlantic Ridge (Hole U1309D; Blackman et al., 2011; Expedition 304/305 Scientists, 2006). The most striking difference is related to the lithologic variability of the two sections. In particular, Atlantis Bank is dominated either by olivine gabbro or oxide-bearing gabbro (only), whereas Atlantis Massif contains a much broader range of lithologies, with a dominant lithology of

Figure F14. Downhole variations in alteration intensity, reddish clay after olivine, magmatic veins, and vein filling minerals, Hole U1473A. A critical point here is that alteration intensity is the sum of several processes affecting cores. For example, plagioclase alteration includes dynamically recrystallized plagioclase (neoblasts), as well as that produced by hydrothermal alteration, which cannot be confidently separated macroscopically, whereas pyroxene and olivine alteration does not include secondary clinopyroxene and olivine, as these cannot be easily separated macroscopically. A key point here is that there is almost no portion of Hole U1473A cores that has not undergone substantial dynamic and/or hydrothermal modification. Alteration intensity: 0 = <3%, 1 = 3%–9%, 2 = 10%–29%, 3 = 30%–59%, 4 = 60%–90%, 5 = >90%. Vein filling proportion: 0 = <10%, 1 = 10%–29%, 2 = 30%–59%, 3 = 60%–90%, 4 = >90%.

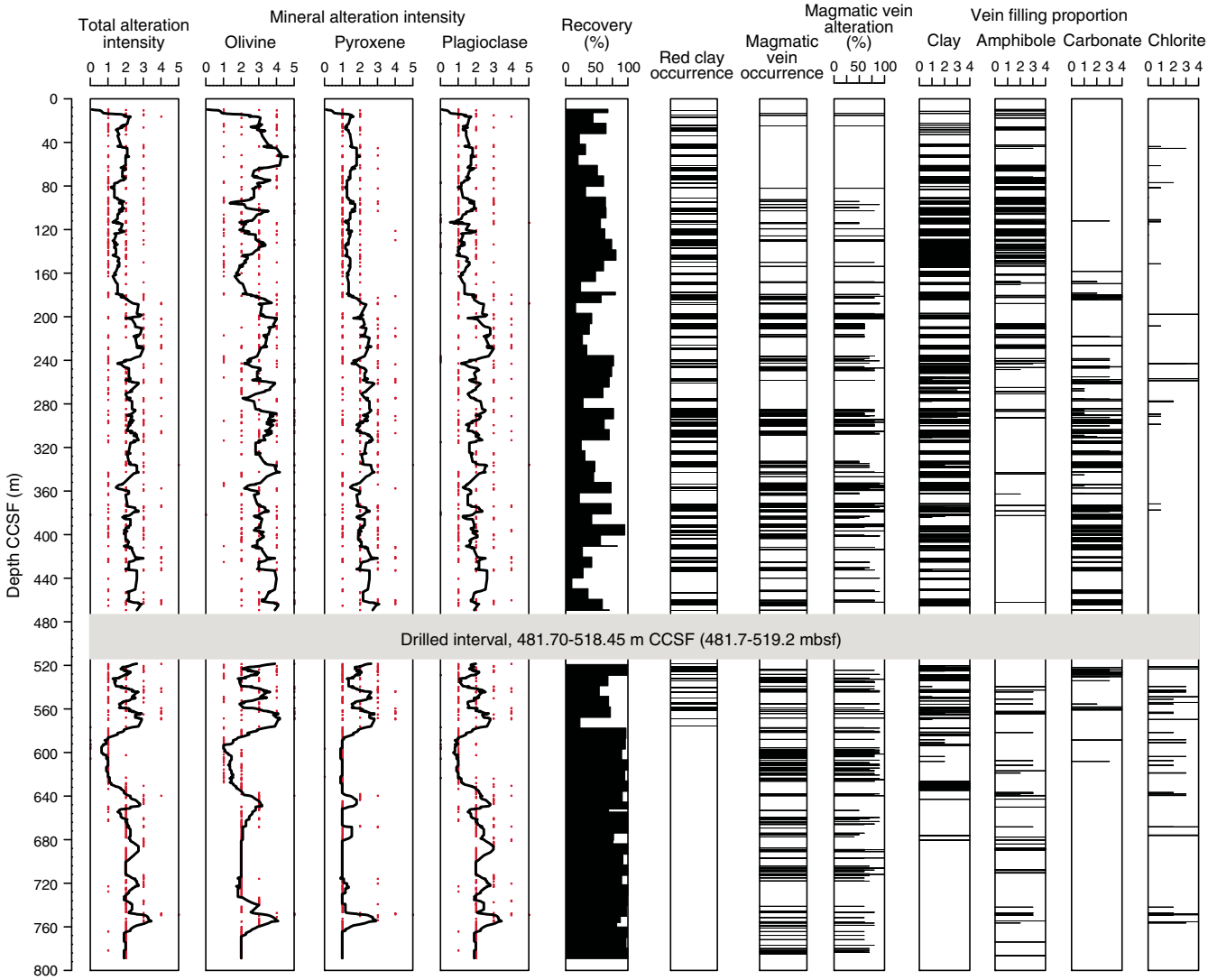

gabbro (sensu stricto; Figure F12) rather than olivine gabbro and lesser amounts of olivine gabbro and oxide gabbros. An even more significant difference is the abundance of troctolite and the presence of relict mantle peridotite horizons in Hole U1309D. Particularly significant are olivine-rich troctolites formed by reaction of mantle peridotite with basalt melt (e.g., Drouin et al., 2009), as well as minor dunite between the gabbro bodies, which were not found at Atlantis Bank. These major differences in igneous stratigraphy at Atlantis Bank and Atlantis Massif demonstrate that significant variability exists in the mode of accretion and internal differentiation of magmatic bodies in the lower crust between oceanic core complexes, likely reflecting variations in magma supply and accompanying tectonic setting, spreading rate, and thermal regime along ocean ridges.

Metamorphic petrology

Hole U1473A gabbros show three distinct modes of alteration: (1) static hydrothermal alteration, (2) alteration associated with crystal-plastic deformation, and (3) alteration associated with cataclastic deformation. Overall, the mineral assemblages in Hole U1473A range from a high-temperature granulite to amphibolite facies assemblage, lower temperature greenschist to zeolite facies, and very low temperature alteration principally including carbonates and clays and mixed-layer smectites. In this, the alteration assemblages are very similar to Holes 735B and 1105A (Dick et al., 1991a, 2000; Pettigrew, Casey, Miller et al., 1999).

Static background alteration in Hole U1473A is pervasive, with alteration mineral abundance estimated from macroscopic description ranging from <3% to 90% (Figure F14). Although alteration mineral abundance may locally exceed 60% in intervals of intense veining or faulting (4% of Hole U1473A cores), in 78% of cores background alteration mineral abundance is <30%. This is very similar to the figure for Hole 1105A (83% of cores contain <30% background alteration). Holes U1473A and 1105A appear to be more altered overall than Hole 735B. Although directly comparable quantitative data are not currently available for Hole 735B, Dick et al. (2000) re-

port long intervals with <5% background alteration for the lower 1000 m of the hole, and, notably, greenschist facies alteration is near-absent throughout (Dick et al., 1991a, 2000).

Static alteration minerals in Hole U1473A consist mainly of (i) colorless amphibole, talc, serpentine, and clay minerals after olivine; (ii) secondary clinopyroxene and brown to green or colorless amphibole after clinopyroxene; (iii) colorless amphibole and talc after orthopyroxene; and (iv) secondary plagioclase and chlorite after primary plagioclase. These minerals occur in different abundances in each core or hand specimen and indicate variable temperature conditions for alteration. Textural relationships document overprinting of lower temperature over higher temperature assemblages during the gabbroic sequence cooling. The formation of the secondary clinopyroxene and brown amphibole association most likely took place at near-solidus temperatures (>800°C). Brownish green and green amphibole and tremolite/actinolite + chlorite ± talc assemblages formed at amphibolite to greenschist facies metamorphic conditions (700°–400°C). The assemblage of secondary plagioclase + chlorite + pale green amphibole (actinolite) with minor amounts of zoisite and titanite indicates greenschist facies conditions (450°–350°C). Serpentinization of olivine most likely took place at temperatures in the range 350°–200°C (i.e., lower than greenschist facies alteration but higher than that of clay mineral formation). Clay minerals are the latest products of alteration at lowest temperatures (<150°C). Downhole trends in background alteration correlate with the distribution of metamorphic veins outlined below.

Amphibole veins and amphiboles replacing primary mafic minerals are dominant at shallower levels (<240 m CCSF), as they are in Hole 735B, whereas carbonate or carbonate-clay veins are conspicuous at 180–580 m CCSF (Figure **F14**). Oxidative reddish clay-mineral replacement of primary minerals is also significant from the seafloor to 580 m CCSF. In these intervals, it is common that millimeter-wide veins have alteration halos that are up to centimeters wide. At deeper levels (>580 m CCSF), micro veins filled with chlorite ± amphibole are more abundant than the millimeter-wide veins.

Felsic veins are typically more altered than host gabbros. The most apparent feature is the replacement of primary plagioclase, and sometimes quartz, by secondary plagioclase, which has a characteristic whitish milky appearance and often has fluid inclusions. Together with association of a relatively high abundance of secondary sulfide and patches of clay minerals in these veins, this implies that the felsic veins were pathways for large volumes of hydrothermal fluids, as also found in Hole 735B (Dick et al., 1991a), particularly at lower temperatures (sub-greenschist facies). Local occurrence of biotite in host gabbros is evidence for metasomatic alteration related to felsic vein intrusion.

Much of the Hole U1473A gabbroic sequence has been subjected to crystal-plastic deformation. In the upper portion of the hole, static background alteration of these porphyroclastic and mylonitic rocks tends to be high, with much (green to brown-green) amphibole, making identification of the synkinematic mineral assemblages difficult. Deeper in the hole, where background alteration is typically much less, the plastically deformed rocks are characterized by neoblasts of olivine, plagioclase, and clinopyroxene with minor brown amphibole and Fe-Ti oxide minerals. This mineral assemblage, effectively granulite facies, indicates deformation at near-solidus temperature conditions (>800°C). Lower temperature amphibolite facies crystal-plastic deformation tends to be present in the form of discrete high-strain mylonitic shear zones largely composed of brown-green hornblende and plagioclase. They are commonly associated with local concentrations of Fe-Ti oxides. The amphibolite facies mineral assemblage also occurs in halos associated with amphibole veins, some of which themselves display evidence of minor crystal-plastic deformation (see below). Amphibolite mylonites and amphibole vein halos show cooling of the gabbroic sequence to temperature conditions around the ductile–brittle transition (~700°C).

Intervals recording intense cataclastic deformation have abundant carbonate and brownish clay mineral(s). Clays and carbonates show textural relationships indicative of their simultaneous formation, and some of the carbonates show a signature of plastic deformation. These observations show that cataclastic deformation took place in association with alteration at low temperatures (<150°C).

Structural geology

The internal structure of the Hole U1473A cores reflects a complex interplay of magmatic and tectonic processes that span a broad range of temperatures, from contemporaneous magmatic intrusion and high-temperature crystal-plastic deformation down to late low-temperature brittle faulting. As a whole, Hole U1473A samples a 600 m thick zone of intense crystal-plastic deformation cut by a later brittle high-angle fault zone with a damage zone that extends to ~570 m CCSF. The variety, distribution, and intensity of the preserved structures are consistent with synkinematic exhumation and cooling in the Atlantis Bank oceanic core complex.

Undeformed parts of Hole U1473A cores preserve weakly developed magmatic fabrics defined by the shape-preferred orientation (SPO) of plagioclase crystals and decimeter-scale igneous layering. The transition from magmatic flow to solid-state crystal-plastic deformation is marked by an increase in plagioclase recrystallization and common development of tapered twins and undulose extinction.

Crystal-plastic deformation is extensively developed throughout Hole U1473A, particularly in the top 600 m. In moderate to intense crystal-plastic deformation zones, the relationship of magmatic fabrics to crystal-plastic fabrics (CPFs) is obscured. In detail, the deformation is heterogeneous with meter- to 10 meter–scale zones of dominantly porphyroclastic shear zones (CPF intensity = 3) separated by relatively weakly deformed gabbros. Locally, deformation intensity increases and true mylonitic zones (CPF intensity = 4) can be found at ~200–210 and ~220–230 m CCSF. Rare thin ultramylonites (CPF intensity = 5) are heterogeneously developed and commonly crosscut the porphyroclastic foliation. The dip of the CPFs is typically shallow, in the range 10°–40°, although, locally, the dip can progressively increase and steepen to vertical. Folding of the fabrics is more common in the upper part of the core. Shear sense indicators are dominantly (apparent) reversed, an observation confirmed by analysis of shear sense indicators in thin sections. Even in those intervals that display little or no macroscopically visible crystal-plastic deformation, thin sections generally reveal weak crystal-plastic overprints in the form of narrow zones of incipient plagioclase recrystallization, especially at the boundaries of pyroxene crystals, and pyroxene microfracturing.

Weak to moderate CPFs commonly have strong SPO defined by large elongated plagioclase and pyroxene crystals. Given the limited amount of recrystallization observed, it appears unlikely that ductile deformation could have caused the alignment of the larger crystals. Therefore, it is more likely that plagioclase and pyroxene were originally aligned by magmatic flow and subsequently overprinted by localized crystal-plastic deformation. Additionally, the grain size layering may have acted as a favored planar anisotropy for subse-

Figure F15. Distribution of (A) CPF intensity, (B) CPF dip variation, and (C) CPF shear sense with depth, Hole U1473A. Red lines = raw data, black curves = 5-cell thickness corrected running averages of intensity. CPF intensity: 0 = undeformed, 1 = foliated, 2 = porphyroclastic, 3 = protomylonitic, 4 = mylonitic, 5 = ultramylonitic.

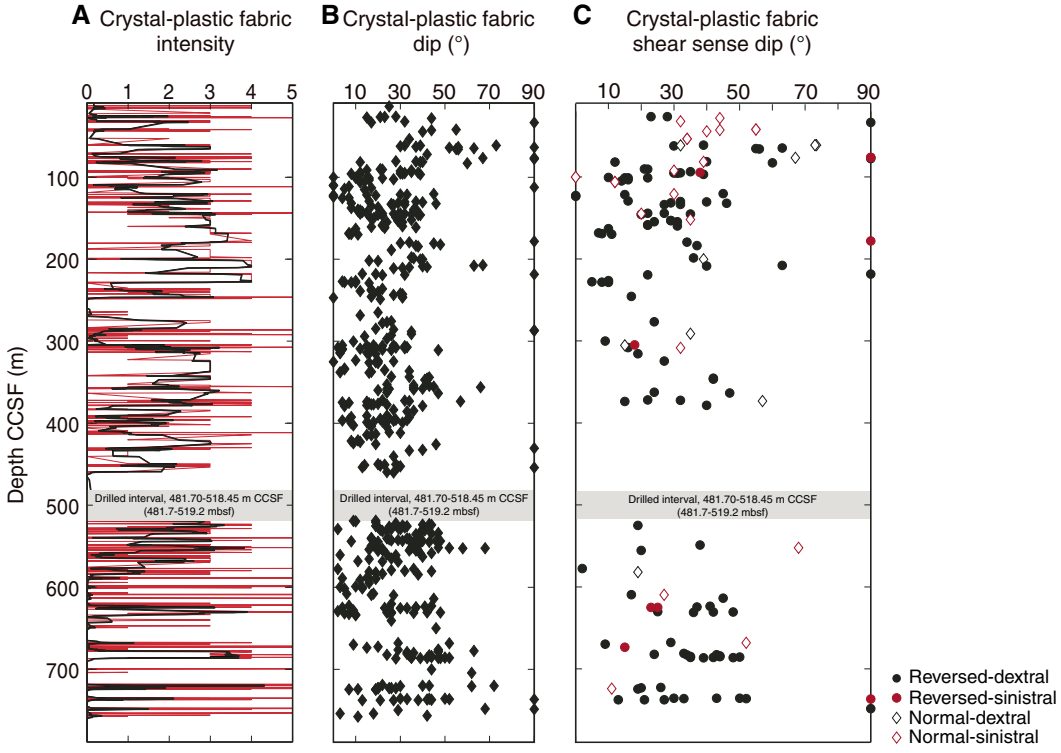

quent CPF to nucleate. In some examples, the layering has a strong crystal-plastic overprint, particularly when the layering has a moderate dip. In other examples, the layering is "necked" and truncated by ductile shear zones.

The conditions over which ductile deformation occurred in Hole U1473A range from near-solidus granulite grade to amphibolite grade (see **Metamorphic petrology**). The distribution of amphibole within mylonites is not restricted to the top of the hole and extends to at least ~670 m CCSF. Several examples of multiple generations of CPFs with variations in shear sense, dip magnitude, dip direction, and metamorphic grade can be observed in Hole U1473A cores. In some examples, the older mylonite has moderate dip and apparent reversed shear sense, whereas the younger crosscutting mylonite has subhorizontal dip and apparent normal shear sense. In others, moderately dipping reversed sense porphyroclastic fabrics are crosscut by subvertical normal sense mylonites. In each case, amphibole is more prevalent in the younger crosscutting fabric. The deformation mechanisms remain the same during granulite and amphibolite grade deformation and are dominated by subgrain rotation recrystallization. This variability in crosscutting relationships indicates a changing strain field through time, with the early CPFs primarily preserving granulite conditions, whereas the younger fabrics reflect amphibolite facies conditions. That the differences in metamorphic facies may be associated with differences in shear zone orientation and shear sense does not accord with the prediction of simple extension at the ridge axis suggests that the lower oceanic crust deformation path is complex and protracted.

Evidence exists for contemporaneous brittle and crystal-plastic deformation. Fractures in clinopyroxene in Hole U1473A gabbros are filled with plagioclase crystals, whereas magmatic ilmenite locally fills cracks in both plagioclase and pyroxene porphyroclasts, indicating that melt was present while fracturing occurred. This can reasonably be anticipated where the crystal/melt ratio is high, as a load-bearing framework can form that can accommodate strain by brittle deformation (Handy et al., 2007). In other examples, plagioclase porphyroclasts have fractures filled with fine-grained recrystallized plagioclase indicating that plagioclase was capable of deforming contemporaneously by brittle (i.e., fracturing) and ductile (i.e., recrystallization) deformation mechanisms. These features have been described in granitoids (e.g., Blumenfeld and Bouchez, 1988) and are interpreted as the transition from magmatic to crystal-plastic conditions, during which submagmatic to crystal-plastic foliations may develop.

Amphibole veins, both brown (hornblende) and pale green (actinolite), exhibit a wide variety of crosscutting relationships with CPFs. Amphibole veins commonly cut crystal-plastic foliation at high angle and may transpose (bend) an older CPF, indicating that vein formation occurred at moderate to high temperatures. In other cases, older CPFs may be simply offset across an amphibole vein, suggesting relatively lower temperature deformation. The relationship between CPFs and veins is complex (Figures **F15**, **F16**). CPFs are overprinted and offset by brittle fractures and local faults with dominantly apparent normal shear sense; however, apparent reversed shear sense is also observed in brittle structures. In most cases, the fractures and faults within plagioclase and pyroxene are filled with amphibole. These microstructural relationships suggest that the brittle-ductile overprint occurred at lower temperatures, mainly ranging from amphibolite to greenschist facies conditions. Some of the shear zones contain Fe-Ti oxides, which are significantly weaker compared to silicate phases (e.g., Till and Moskowitz, 2013). We suggest that discrete parts of the shear zone were still deforming by ductile deformation mechanisms, whereas other zones

Figure F16. Metamorphic vein density and amphibole, clay, and carbonate vein frequency with depth, Hole U1473A. Vein density: 0 = no veins, 1 = <1 vein/10 cm, 2 = 1–5 veins/10 cm, 3 = 5–10 veins/10 cm, 4 = 10–20 veins/10 cm, 5 = >20 veins/10 cm. Black curve = 11-point running average, horizontal dash-dotted lines = fault zone locations.

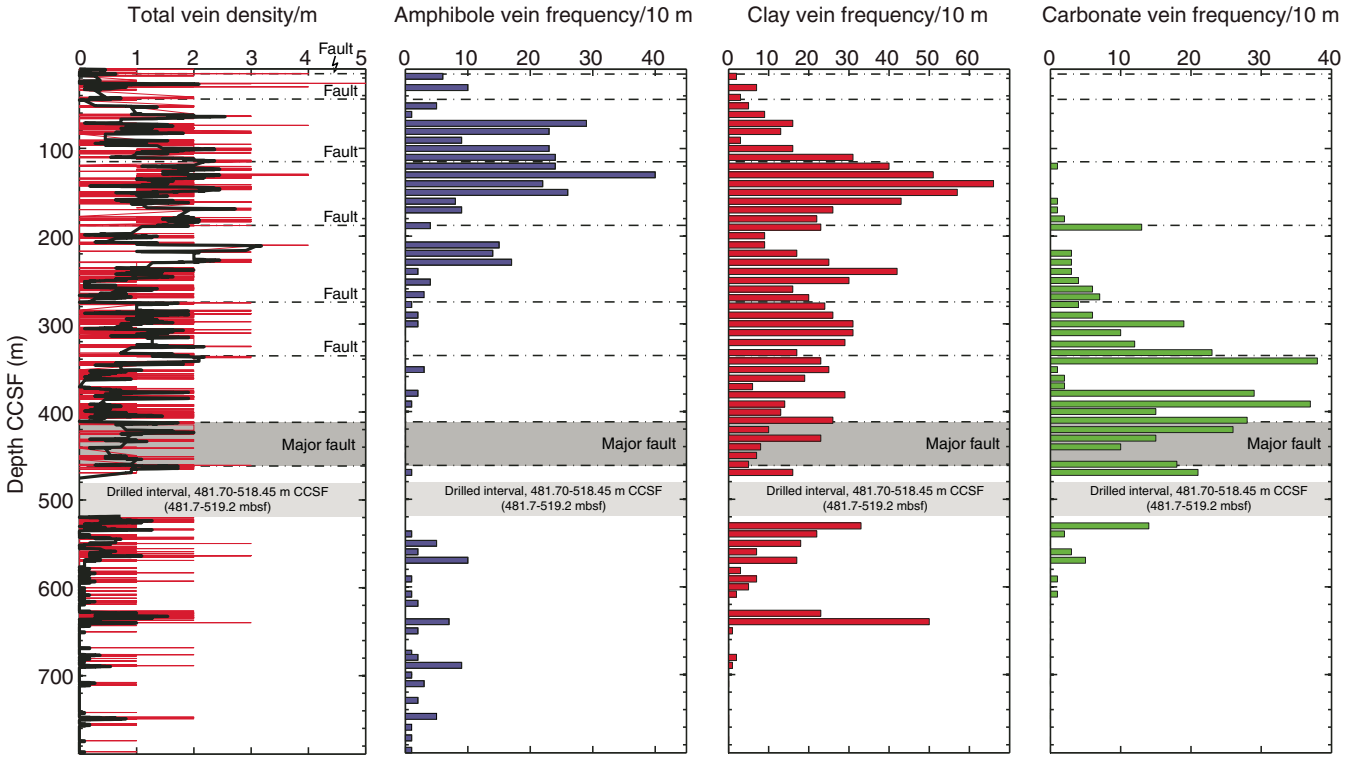

were deforming by fracturing. The resulting microstructures are characterized by coeval ductile and brittle deformation mechanisms that were activated by variations in the thermal gradient, composition, and grain size.

Fe-Ti oxide–rich domains are heterogeneously distributed throughout Hole U1473A, as demonstrated by the distribution of magnetic susceptibility, which is an approximation for the proportion of Fe-Ti oxide minerals (see **Petrophysics**). The relationship between deformation and the presence of Fe-Ti oxides can be cryptic, with examples of Fe-Ti oxides occurring in both deformed and undeformed samples. There are 26 ultramylonite shear zones within Hole U1473A to 789 m CCSF, 18 of which correlate with a peak in magnetic susceptibility. Most susceptibility peaks that do not correlate with the presence of an ultramylonite instead correlate with the presence of a mylonite; however, the two largest contiguous zones of deformation, the 10 m thick mylonites from 201 to 210 m CCSF and from 219 to 228 m CCSF, do not correlate with peaks in magnetic susceptibility and are Fe-Ti oxide poor.

No clear evidence has been found from the cores for crystal-plastic deformation having predated or been contemporaneous with intrusion of the individual geochemically defined coarse olivine gabbro units. However, the felsic veins appear to have been synkinematic: some of the late-magmatic felsic veins were deformed along with the gabbros, whereas others, themselves undeformed, clearly crosscut plastically deformed gabbro. The dikes that cut the Hole U1473A section were intruded under a range of conditions likely ranging from upper amphibolite to sub-greenschist facies conditions; although none exhibited crystal-plastic deformation, the enclosing gabbros generally do. Taken together with the clear relationship between late evolved oxide gabbros and discrete shear zones, it may be concluded that deformation commenced almost immediately after crystallization of the main gabbro body or bodies, whereas late-stage interstitial melts were still present. Continuing deformation led to the exhumation and cooling during extension along a detachment shear zone that formed the oceanic core complex.

Seven discrete fault systems were identified in Hole U1473A based on the presence of fault rocks and fractured intervals (Figure **F17**). They range from discrete 5 cm thick cataclasites at the top of the hole to a major fault zone at 411–469 m CCSF. An eighth discrete fault may exist at ~570 m CCSF; otherwise, no faulted intervals were encountered at greater depths. In each case, the faulted and fractured zones correspond to intervals of borehole enlargement, reduced core recovery, increased penetration rates, and in some instances to drilling difficulties (see **Operations** in the Site U1473 chapter [MacLeod et al., 2017b]). The 50 m thick fault zone at 411–469 m CCSF consists of chlorite-rich and carbonate-rich breccias and correlates with an increase in carbonate veining. Taken in conjunction with evidence for a negative temperature anomaly in downhole logs from this depth (see **Petrophysics**), it appears that the fault zone controls an active hydrologic system. Carbonate veining is positively correlated with fault rock intensity in most of the faulted intervals above and below the 411–469 m CCSF fault zone (Figure **F16**). The downhole frequency of carbonate veins increases toward the major fault zone and then decreases below it, correlating with the damage zone of the fault as defined by the fracture density of the rocks (Figure **F17**). The background alteration and olivine alteration increases with the degree of carbonate veining, suggesting that low-temperature olivine alteration is enhanced in the vicinity of carbonate veins. This is supported by macroscopic core observations displaying the pronounced red-stained (oxidative) alteration of olivine in the vicinity of the carbonates (see **Metamorphic pe-**

Figure F17. Fault rock intensity (1 = minor fracturing, 2 = moderate fracturing, 3 = incipient breccia, 4 = fault breccia, 5 = cataclasite) and fracture density (1 = 1 fracture/10 cm, 2 = 1–5 fractures/10 cm, 3 = >5 fractures/10 cm) with depth in Hole U1473A, raw data plotted. Fault rock intensity and fracture density are plotted as 11-cell (10 cm interval per cell) running averages (black curves). Red lines = raw fault rock intensity data, gray bars = seven major fault systems.

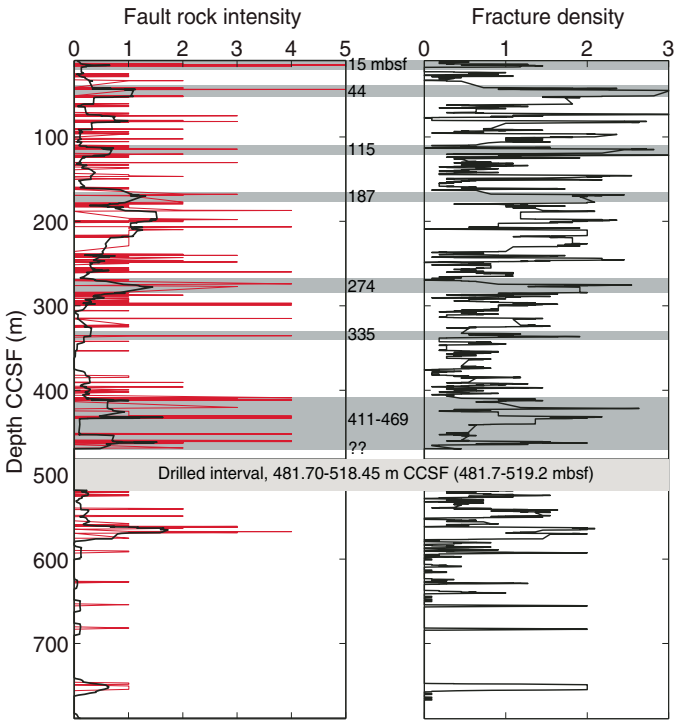

trology). These smaller fault zones may too be the focus of active fluid flow.

The following are the main structural conclusions from Hole U1473A:

- Multiple generations of felsic veins, most with a crystal-plastic overprint, provide evidence for a protracted history of melt generation and deformation.
- Hypersolidus magmatic fabrics and grain size layering provide anisotropies that preferentially cause the nucleation of CPFs.
- A 600 m thick zone of intense crystal-plastic shearing (Figure **F15**) represents high-temperature deformation related to formation of the Atlantis Bank oceanic core complex and associated detachment fault zone; however, we cannot correlate it directly with the deformed interval at the top of Hole 735B.
- Multiple generations of CPFs with different orientations, shear sense, and metamorphic grade attest to a protracted history of ductile deformation.
- Shear sense is predominantly normal in the upper 50 m of Hole U1473A but tends to be reversed at greater depths. This same observation is made in Hole 735B but with the difference that the transition in the latter occurs at ~450 mbsf.
- A strong correlation exists between the presence of Fe-Ti oxides and that of mylonite, ultramylonite, and magmatic contacts; however, the modal abundance of Fe-Ti oxide does not seem to correlate with deformation, and weaker CPFs tend not to correlate with the presence or absence of Fe-Ti oxide.
- The transition from crystal-plastic to brittle deformation is associated with granulite to amphibolite and, in some cases, greenschist facies alteration by way of ductile, semibrittle, and brittle deformation mechanisms. The degree of greenschist grade deformation is, however, much less in Hole U1473A than in Hole 735B and in previously reported sample suites from the surface of Atlantis Bank (e.g., Miranda and John, 2010).
- Amphibole veins are concentrated in the upper 400 m of Hole U1473A (Figure **F16**) and either deflect or offset older CPFs at a high angle. Brittle overprint of high-temperature CPFs is relatively limited and restricted to the upper ~300 m of the hole.

A 50 m thick high-angle fault zone, defined by several fault breccias, carbonate vein abundance, enlargement in borehole size, and reduction of in situ borehole resistivity, occurs from 411 to 469 m CCSF. A temperature anomaly associated with this zone suggests the fault is hydrologically active. Six other smaller fault zones are identified at shallower levels within Hole U1473A (Figure **F17**). All corresponded to lowered core recoveries, increased penetration rates, and, in some cases, problematic drilling conditions.

Geochemistry

The Hole U1473A lithologies are dominated by moderately evolved olivine gabbro with Mg# between 82 and 66. Mg# co-varies with other petrogenetic indicators such as Ca#, Ti, Y, Cr, and Ni. The variations in Cr and Ni concentrations cannot be explained by modal mineralogy but are attributed to the composition of pyroxene and olivine in the rock.

Downhole variation plots show major discontinuities in Mg#, Cr and Ni contents, and Ca# at ~60–90, 300, and ~700 m CCSF (Figure **F13**). The discontinuities are interpreted as delineating upwardly evolving units of magma intruded in individual intrusive events. The nature and scale of the discontinuities are remarkably similar to those seen in Hole 735B (Figure **F6**) (Dick et al., 2000) and are interpreted in a similar manner. In addition to these major-scale variations, however, oxide gabbros occur in centimeter-scale intervals throughout the section. These are significantly more evolved than the background olivine gabbro and provide evidence for the migration of late-stage melts over minimum distances of tens to hundreds of meters.

The average composition calculated for Hole U1473A is very similar to that of Hole 735B, with Mg# of 71 ± 3 and TiO_2 of 0.7 ± 0.2 wt%. The average composition of the Atlantis Bank gabbros is slightly more evolved than that of Atlantis Massif (Hole U1309D; Godard et al., 2009), although their standard deviations overlap. They are both, however, substantially more fractionated than the bulk lower crust average calculated for Hess Deep (fast-spread lower crust) by Gillis et al. (2014), although we note that the Hess Deep calculation is based on extrapolation from relatively short drilled sections and thus is only an approximation of the composition of the East Pacific Rise lower crust.

Hole U1473A gabbros have H_2O contents of 0.2–8.0 wt% (mean = 1.0 ± 0.9 wt%, median = 0.8 wt%), much higher than expected in pristine cumulates. Even petrographically fresh samples (thin section alteration intensity = 0–2) have mean H_2O contents of 0.8 ± 0.6 wt% (median = 0.7 wt%). H_2O abundance decreases with depth and is therefore likely to be controlled mostly by deep and near-pervasive infiltration of seawater through the crustal section. Examination of altered and fresh sample pairs indicates that the alteration did not significantly alter major or trace element concentrations. This is consistent with the infiltration of low-salinity seawater-derived fluids with limited potential for mobilizing other elements.

CO_2 is below detection limit in many of the samples, but concentrations of up to 2 wt% were obtained for altered rocks in the

carbonate-veining zone (~210–580 m CCSF). An unexpected result was that four of the carbonate-rich samples investigated are dominated by up to 0.5 wt% of inorganic carbon rather than CO_2. These high concentrations are similar to the range reported for clay-rich alteration of glass on the seafloor and may be related to clay alteration in the gabbros. The amount of organic carbon present is a factor of 10 higher than determined for the majority of serpentinites investigated previously. This is an intriguing result and may require that low-temperature alteration minerals of gabbro be added to the list of potential microbial habitats in the subseafloor.

Microbiology

Microbiological sampling during Expedition 360 focused on exploring evidence for life in the lower crust and hydrated mantle using culture-based and culture-independent approaches, microscopy, and enzyme assays. Sampling focused on cores with evidence of alteration or fracturing within all lithologies encountered. In total, 68 whole-round samples (4–22 cm long) were collected for microbiological analysis. Adenosine triphosphate (ATP) was quantified from all samples and ranged from below detection to 5 pg/cm^3 (mostly <1 pg/cm^3), indicating the presence of a subsurface biosphere in Atlantis Bank. Samples collected for postcruise research include fixed samples for cell counts to quantify microbial biomass and frozen samples for DNA, RNA, and lipid extraction to describe the diversity (DNA and lipids) and activity (RNA) of the microbial community. A total of 38 samples were inoculated into as many as 10 different kinds of microbial media targeting specific prokaryotic iron-reducing microbes, sulfate-reducing bacteria, sulfur-oxidizing microbes, archaeal methanogens, and eukaryotic fungi. These will be analyzed during postcruise research. In addition, for 12 samples we established nutrient addition experiments testing nutritional constraints on microbial biomass in this environment. Enzyme activity assays were conducted using substrates for alkaline phosphatase, leucine aminopeptidase, and arginine aminopeptidase at 15 sample depths in Hole U1473A. These experiments are ongoing, but initial analysis indicates the presence of very low alkaline phosphatase activity, whereas enzyme activity for both peptidase substrates was below detection.

Finally, a new microbial contamination tracer, perfluoromethyldecaline (PFMD), was used for contamination testing for the first time. PFMD was run during coring operations for 10 samples and was routinely detected in the drilling fluids, usually on the outside of uncleaned cores, and rarely above detection on the outside of cleaned cores. It was below detection on the inside of cores, indicating that penetration of drilling fluids to the interior of whole-round drill cores where we collected our samples is unlikely. We ran three runs of the commonly used tracer perfluoromethylcyclohexane (PMCH) at the end of the cruise for comparison. It was more difficult to clean the core exteriors successfully with this more volatile tracer, and PMCH was detected on occasion on core interiors.

Paleomagnetism

Remanence measurements made on archive section halves from Hole U1473A generated demagnetization data at more than 12,000 measuring points downhole. Virtually all intervals have positive inclinations indicating that the gabbros hold a reversed polarity magnetization, consistent with the interpretation of marine magnetic anomalies (Allerton and Tivey, 2001) that place Hole U1473A within geomagnetic polarity Chron C5r.3r (Gradstein et al., 2012). Moreover, the gabbros carry sufficiently strong magnetizations to account for the observed magnetic anomalies over Atlantis Bank.

The archive section-half data were subject to principal component analysis (PCA) using a processing and filtering scheme designed to rapidly identify the highest quality highest coercivity components for subsequent tectonic interpretation. The resulting principal component data allow division of the hole into upper and lower zones with statistically different inclinations (Figure **F18**). Thermal demagnetization data from discrete samples subject to the same filtering for reliability support this division. The boundary between major inclination zones corresponds to the fault zone observed at 411–469 m CCSF, from a mean value of ~72° shallower than 403 m CCSF to a mean value of ~61° deeper than 403 m CCSF. A narrow zone of steeper inclinations (mean = 73.3°) is also seen between 734 and 750 m CCSF. Compared to the expected dipole inclination of 51.3°, these results imply a significant but variable rotation of the Atlantis Bank footwall since acquisition of magnetization, with the major change across the fault zone likely reflecting differential rotation across this structure.

Figure F18. Summary of inclination data from Hole U1473A based on quality-filtered principal components determined from 25–50 mT alternating field demagnetization data before (green) and after (orange) piece averaging. Red dashed line = geocentric axial dipole. The data define five distinct inclination zones, whose potential origins are discussed in the text.

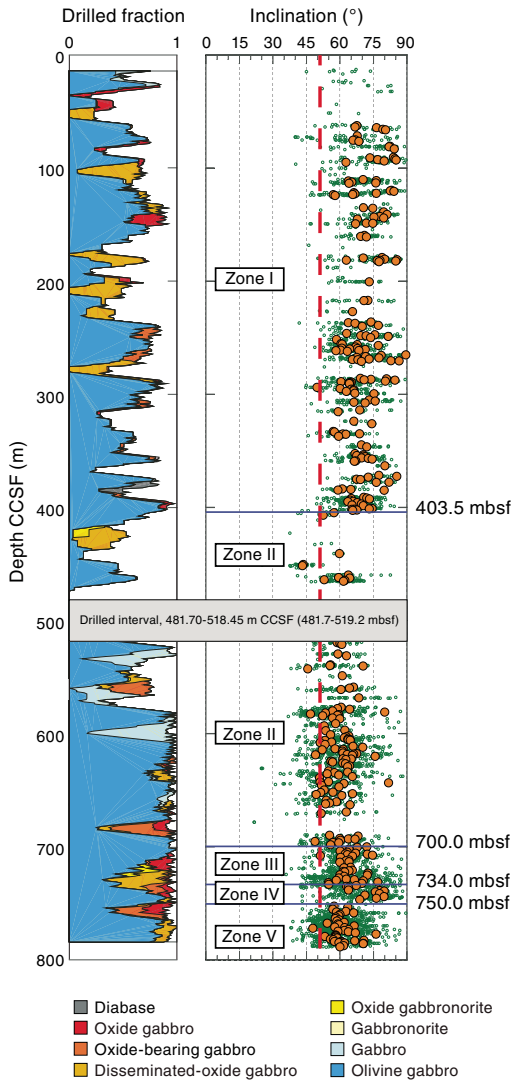

Although the greater part of Hole U1473A carries reversed polarity magnetization, thermal demagnetization of discrete samples and alternating field demagnetization of archive section-half pieces reveals characteristic remanences with negative inclinations in some narrow zones of altered gabbro (around ~564, 678, and 749 m CCSF). The presence of these zones within broader intervals of reversed polarity indicates (near-) complete remagnetization of these rocks during a subsequent normal polarity period. The timing of the alteration cannot be uniquely determined from these data, but the presence of these components in the lower part of the hole suggests that the reversal boundary between reversed geomagnetic polarity Chron C5r.3r and normal polarity Chron C5r.2n may occur in close proximity to the current bottom of Hole U1473A.

Petrophysics

Core sections were measured using data loggers for magnetic susceptibility, gamma ray attenuation (GRA) density, and natural gamma radiation (NGR). Magnetic susceptibility was measured on both whole-round sections and archive halves, using a pass-through sensor coil and a contact probe, respectively. The measured magnetic susceptibility varies over the whole instrument range (10,000 instrument units [IU]; i.e., ~0.1 SI); high magnetic susceptibility values (>1,000 IU) are ubiquitously related to abundant magnetite in gabbroic lithologies. The dominant olivine gabbro lithology has relatively low susceptibility that does not exceed a few hundred instrument units. At the centimeter to decimeter scale, high values of magnetic susceptibility indicate oxide-rich intervals, seams, and patches.

NGR from the gabbro cores is consistently very low (≤1 count/s). Several isolated peaks up to ~10 counts/s were observed in the vicinity of felsic veins. In the lower part of the hole (deeper than ~575 m CCSF), these narrow peaks often correlate with the highest magnetic susceptibility signals, indicating the presence of magnetite in the felsic veins.

GRA density estimates range from 2.1 to 3.2 g/cm^3 and average ~2.65 g/cm^3. Estimates are slightly less variable in the bottom of the hole (below the major fault zone at ~411–462 m CCSF) than in shallower sections, with an average value of about 2.67 g/cm^3.

Density and porosity were determined for 186 samples. Grain density ranges from 2.88 to 3.13 g/cm^3 and averages 2.98 g/cm^3. It does not vary significantly downhole, except for a slightly higher variability above the major fault zone at ~411–469 m CCSF. Porosity is generally very low; it ranges from 0.1% to 4.2% and averages 0.6%.

Compressional seismic velocity was measured at room pressure and temperature along three mutually perpendicular directions on 2 cm × 2 cm × 2 cm cubic samples. A total of 184 gabbroic samples from Hole U1473A were measured, 94% of which were olivine gabbro. V_P ranges from 5930 to 7150 m/s, with an average of 6734 m/s and an average standard deviation of 25 m/s. Above the major fault zone at ~411–469 m CCSF, V_P shows a modest increasing trend over the interval ~280 to ~400 m CCSF, from ~6700 to ~7100 m/s. This progressive increase does not continue deeper in the hole. Below the major fault zone, V_P is lower on average (6646 m/s) than in the upper part of the hole (6795 m/s), with a similar range of local-scale variability. Local trends of decreasing V_P over a few tens of meters match trends of increasing porosity and correspond to more fractured intervals and fault zones. The measured apparent anisotropy of V_P is generally low, ranging from 0.1% to 10.9% and averaging 2.2%; the slowest average V_P of the three measured directions is parallel to the core axis (~6708 m/s).

Thermal conductivity was measured on 86 samples from archive halves. It ranges from 1.77 to 2.52 W/(m·K) and averages 2.28 W/(m·K). The standard deviation of the measurements is <2% (0.66% on average). Olivine gabbro conductivities are in the same range as those measured during previous oceanic crust drilling expeditions. Deeper than ~450 m CCSF, the average thermal conductivity is slightly higher (2.36 W/[m·K]) than in the upper part (2.21 W/[m·K]). This may partly reflect the general change in background alteration at the bottom of the hole; deeper than 570 m CCSF, olivine is less altered and secondary clays are absent (Figure **F14**).

Downhole logs were successfully acquired at the end of drilling operations using three tool strings: a modified "triple combo" (NGR spectroscopy, bulk density, bulk resistivity, and magnetic susceptibility), a Formation MicroScanner-sonic string (seismic velocity and electrical resistivity borehole wall imaging), and an Ultrasonic Borehole Imager string (acoustic borehole wall imaging). Each tool string also measured total NGR and borehole temperature. The borehole diameter measured by the triple combo tool string shows significant variations in the upper part of the hole to ~570 m wireline log depth below seafloor (WSF) and a much more regular and clean shape deeper, where core recovery averaged 96%. Intervals where the hole diameter is very variable and/or out of gauge correspond to low recovery and/or faulted material identified in the core. The presence of fault zones at ~411–469 m CCSF is indicated by low electrical resistivity and low bulk density. A negative temperature excursion recorded by the temperature tool on each run also places the base of a major fault that introduces colder fluid into the borehole at ~469 m WSF.

In the bottom part of the hole (deeper than ~570 m CCSF), V_P averages about 6840 m/s, significantly higher than shallower than 570 m CCSF, where it is generally about 6300–6400 m/s away from fault zones.

Hole 1105A redescription

During the 11 day transit from Colombo, Sri Lanka, to Site U1473 at Atlantis Bank, the Expedition 360 science party reexamined cores drilled during Leg 179 in Hole 1105A (Pettigrew, Casey, Miller, et al., 1999; Casey et al., 2007). This activity involved rigorously describing the cores and many of the accompanying thin sections with the primary purpose of familiarizing the science party with the material likely to be encountered at the new Site U1473, situated 1.4 km to the north. The science party developed templates for the description of the igneous, metamorphic, and structural features of the cores and thin sections to establish core description protocols for Site U1473 cores. An additional benefit of redescribing Hole 1105A cores is that the data generated are in a format directly comparable with those for Hole U1473A.

In general, our findings were very similar to those produced by the Leg 179 scientists; however, with a larger science party to work on the cores, some of the information collected is new. We include this information in the **Hole 1105A redescription** chapter (MacLeod et al., 2017a), as a basis for direct comparison with the results of drilling at Site U1473. In addition, we were able to make certain physical properties measurements on Hole 1105A cores, including section-half magnetic susceptibility measurements, that had not been possible during Leg 179. It is important to note here that the observations made on the Hole 1105A cores by the Expedition 360 scientific party augment rather than replace those made by the Leg 179 scientists.

Igneous petrology

Our observations on the igneous petrology of this section are summarized below and then briefly compared with those made during Leg 179. The 30 cores recovered from Hole 1105A are composed of gabbroic rocks and related felsic veins (Pettigrew, Casey, Miller, et al., 1999; Casey et al., 2007). The gabbroic rocks are mostly coarse grained with subophitic to granular textures and are variably deformed. Subophitic textures dominate in undeformed samples. The main lithologies are oxide gabbro and olivine gabbro, followed in abundance by gabbro (sensu stricto). A significant proportion of the olivine gabbro and gabbro intervals contain small amounts of oxides and are referred to as disseminated-oxide gabbro (1%–2% oxides) and oxide-bearing gabbro (2%–5% oxides). On the whole, gabbroic rocks with oxides >1% are dominant deeper than 35 m CCSF, and they tend to be more plastically deformed than other lithologies. Oxides are particularly abundant and probably crystallized from percolating evolved melts. In these deformed gabbros, oxides are not obviously affected by plastic deformation, and thus apparently crystallized after dynamic recrystallization of the silicates. Some rare undeformed oxide gabbros are also observed. Thin intrusions of fine-grained olivine gabbro occur between 60 and 75 m CCSF. Numerous felsic veins occur throughout the core and are concentrated at 15–65 and 138–158 m CCSF. Detailed observations of the corresponding thin sections allow us to document the evolution of late-stage melts within a crystallizing mush and to track the origin of magmatic oxide minerals where they are particularly enriched.

When compared with Hole 735B gabbros (Robinson, Von Herzen, et al., 1989; Dick, Natland, Miller, et al., 1999), Hole 1105A is more enriched in oxide-bearing varieties (disseminated-oxide gabbro, oxide-bearing gabbro, or oxide gabbro) and therefore represents a section of crust that is more evolved overall than that recovered in Hole 735B. The oxide-rich section of Hole 1105A is both thicker and more enriched in oxides than the principal oxide-rich portions of Hole 735B (Units III and IV; 170.2–274.1 mbsf). Deformation grade and alteration patterns are also different, and a downhole differentiation trend similar to that observed for Hole 735B oxide gabbro is questionable for Hole 1105A whole-rock compositions but may be more evident when considering mineral compositions (Dick, Natland, Miller, et al., 1999; Dick et al., 2002; Pettigrew, Casey, Miller, et al., 1999; Casey et al., 2007). If the Hole 1105A section is equivalent to any portion of Hole 735B, the most likely candidate would be Units III and IV (170.2–274.1 mbsf; Casey et al., 2007). Nevertheless, given the mismatch in comparisons presented above and as discussed in Casey et al. (2007), it is probable that Hole 1105A does not represent a single layer connected directly with Hole 735B; rather, it may instead record the manifestation of a similar process, dominated by the percolation of evolved melts that have the potential to precipitate oxides and concentrate them in high-porosity regions located in the shallowest levels of the sections. In Hole 735B, these regions clearly correspond to units affected by crystal-plastic deformation; however, such a relationship is less evident in Hole 1105A. The shallowest section of Hole 1105A (15–40 m CCSF) is composed of material that is less evolved (olivine gabbro) and less deformed than in the deeper sections and is similar to several units recovered lower in Hole 735B. In Hole 735B, most felsic veins are associated with oxide gabbro (e.g., Natland et al., 1991), a relationship that is not observed in Hole 1105A.

When compared with results of Leg 179 (Pettigrew, Casey, Miller, et al., 1999), we have defined fewer intervals: 108 during Expedition 360 versus 141 during Leg 179. Their modal content estimates are on average also quite different from ours, resulting in different proportions of rock types (olivine gabbro was 39% during Expedition 360 versus 43% during Leg 179, gabbro was 21% versus 36%, respectively, and oxide gabbro was 41% versus 21%, respectively). Our values as presented above have been adjusted to match Leg 179 descriptions, since during Leg 179 disseminated-oxide gabbro (defined as having oxide content from 1% to 2%) and oxide-bearing gabbros (oxide content from 2% to 5%) were included within the gabbros.

The units defined for Hole 1105A during Leg 179 and Expedition 360 are relatively similar to each other. Four units were defined both during Leg 179 (two subunits in Unit II) and during Expedition 360. The transition between Units I and II are relatively close (<10 m difference), the transition between Units IIA and IIB of Leg 179 and between corresponding Units II and III of Expedition 360 also differ by <10 m, and the transition between Units IIB and III of Leg 179 is 4 m deeper than the transition between Units III and IV of Expedition 360. Leg 179 scientists also defined a Unit IV in the deepest part of Hole 1105A, but this distinction was not made during Expedition 360.

Metamorphic petrology

Most gabbros in Hole 1105A (83%) have <30 vol% of secondary minerals formed by static alteration; intervals of extensive static alteration (≥60 vol%) are rare (<3% of the total). The intensity of static alteration shows no trend with depth in the hole. Olivine and plagioclase are generally the most and the least altered phases, respectively. Plagioclase is substantially altered only where the host rock shows intense veining or cataclasis. Felsic veins tend to be substantially more altered than their host gabbros.

High-temperature alteration is largely associated with crystal-plastic deformation. The neoblastic minerals (plagioclase, olivine, and clinopyroxene, the latter locally associated with minor brown amphibole) document crystal-plastic deformation under granulite to upper amphibolite facies conditions. The high-temperature alteration is also locally manifested by static replacement of magmatic clinopyroxene by secondary clinopyroxene and minor brown hornblende.

Subsequent phases of metamorphism are recorded in veins and by static alteration minerals. Veins filled with brownish green hornblende forming up to 1 mm long crystals are presumed to have formed under amphibolite facies conditions. Other veins are characterized by pale green actinolitic amphibole needles associated with chlorite. These veins likely developed under greenschist facies conditions.

The moderate-temperature static alteration minerals vary in conjunction with the primary mineral. In particular, variable replacement modes were observed for olivine. Olivine is commonly altered to talc and minor oxide aggregates, frequently with an outer rim of chlorite where it is in contact with plagioclase. A less frequent mode of olivine alteration is represented by local aggregates of chlorite and pale green amphibole in coronae along plagioclase contacts. Clinopyroxene is altered along rims, cleavage surfaces, and micro veins into green to pale green amphibole. Plagioclase hydrothermal alteration is mostly confined to development of chlorite along the contacts with primary mafic minerals and within micro veins, in many instances in association with minor secondary plagioclase.

Abundant veins filled with clay minerals record hydrothermal alteration under oxidative sub-greenschist facies conditions. Veins of this type are conspicuous in a few intervals in association with significant cataclastic deformation. In these intervals, olivine and pyroxene are mainly replaced by reddish brown clay minerals or by

mixtures of clay and iron oxyhydroxides. Similar clay and carbonate veins and brownish clay pseudomorphs after olivine and pyroxene occur in host gabbros near the cataclastic zones. Low-temperature carbonate veins are also present toward the bottom of Hole 1105A.

Structural geology

The distribution and intensity of structures in Hole 1105A—magmatic contacts, veins, and fabrics; CPFs; alteration veins; cataclastic material; and fractures—represent a continuous record of deformation from ductile to brittle. The proportion and overall intensity of gabbroic rocks displaying CPFs increases downhole, from decimeter-thick discrete mylonites in the top 80 m CCSF to meter-thick gneissic porphyroclastic shear zones deeper than 80 m CCSF. Intervals of mylonite and ultramylonite, which may overprint earlier magmatic fabrics, are characterized by elongated bands of plagioclase intercalated with bands of pyroxene and are commonly Fe-Ti oxide rich. CPFs are shallowly to moderately inclined and commonly display reversed shear sense, although normal shear sense does occur. Fe-Ti oxides are abundant in many samples, ranging from deformed to undeformed, and concentrate near magmatic contacts. Eighty percent of magnetic susceptibility peaks correlate with intervals that contain some evidence for crystal-plastic deformation.

Magmatic fabrics (shape-preferred primary orientations of elongate crystals) are commonly overprinted and obscured by subsequent CPFs. Where magmatic fabrics are recognized they are weakly developed. Typically, they are inclined and better developed in finer grained rocks and near magmatic contacts. Magmatic contacts range from intrusive to gradational and sheared, with the majority of contacts being gradational, defined by grain size or modal variations. Magmatic veins are common throughout the top and bottom of Hole 1105A (15–65 and 138–158 m CCSF) and are absent from the middle part of the section (65–138 m CCSF). Most of the magmatic veins crosscut a previous CPF and are not themselves plastically deformed; however, in a few instances leucocratic gabbroic veins are observed that have a mylonitic overprint. In some cases, deformation is confined to the vein, whereas the host gabbro is apparently undeformed. These intrusive relationships indicate at least two generations of melt input and deformation. The distribution of magmatic vein dips is bimodal, similar to that seen in Hole 735B.

Five fractured zones are identified in Hole 1105A, two of which are fault zones. These fault zones (at 112 and 127 m CCSF) are each ~5 m thick fractured intervals surrounding a core of fault breccia. Discrete fractures are generally planar, some with slickensides. The slickenlines have a steep to moderate rake, indicating oblique to dip-slip. The dip magnitude distribution is not random.

Alteration veins vary in orientation as well as mineralogy: amphibole veins tend to be moderately to steeply inclined, whereas carbonate and clay veins are generally subhorizontal. Amphibole veins are most common at 40–50, 60–70, and 120–130 m CCSF, intervals in which other vein fills are rare. Incomplete fill of calcite and clay veins and the correlation of these veins with zones of fracturing are indicative of low-temperature, potentially recent fluid flow through the fracture systems. This is consistent with measured downhole logging temperature anomalies at 104–105 and 135–136 mbsf (Pettigrew, Casey, Miller, et al., 1999).

The relative ages, distributions, and orientations of structures, ranging from magmatic contacts to brittle faults, document a down-temperature continuum of deformation, spanning the entire history from magmatic accretion to exhumation. Perhaps the most striking observation is the absence in Hole 1105A of a coherent high-strain porphyroclastic to mylonitic shear zone at the seafloor directly comparable to that documented in Hole 735B 1.2 km to the east-northeast (Robinson, Von Herzen, et al., 1989; Dick et al., 1991a). Given the generally accepted interpretation of Atlantis Bank as an oceanic core complex (see **Summary**), the apparent absence of detachment fault shearing at the surface of the platform might best be explained by erosion following the earlier uplift of Atlantis Bank to sea level. Erosion might also explain the absence of a significant brittle overprint at the top of the hole. Most likely, the high-temperature deformation exhibited in Hole 1105A represents a slightly deeper part of the damage zone related to the detachment shear zone below the ridge axis.

Paleomagnetism

Remanence measurements were made on archive halves from Hole 1105A. These had previously been demagnetized at a maximum field of only 20 mT during Leg 179; hence, during Expedition 360 we were able to conduct further stepwise demagnetization up to 50 mT. We thereby generated demagnetization data at >2500 measurement points downhole. These data were subject to PCA using a processing and filtering scheme designed to rapidly identify the highest quality demagnetization data for subsequent tectonic interpretation. Piece-averaged principal components have a mean inclination of 72.5° (determined from 346 archive-half pieces). This value is in good agreement with those obtained previously in Hole 735B (71.1°) and from seabed rock drill samples (Allerton and Tivey, 2001). Compared to the expected dipole inclination of 51.3°, the results imply a consistent minimum rotation of the Atlantis Bank footwall of ~20° since acquisition of magnetization.

Petrophysics

New physical properties measurements on section halves and section-half pieces from Hole 1105A were acquired and integrated with the new shipboard core descriptions. Using equipment not available to Leg 179 scientists, we measured point magnetic susceptibility on archive halves and thermal conductivity on discrete samples.

The mean magnetic susceptibility of rocks recovered in Hole 1105A is 1800 IU (i.e., ~1800 × 10^{-5} SI). Several intervals have susceptibility much greater than the average value for Hole 1105A and correspond to intervals with a higher abundance of magnetite in oxide or oxide-bearing (olivine) gabbro.

Thermal conductivity was measured on 28 gabbro pieces taken at irregularly spaced intervals along Hole 1105A. Measured values range from 1.804 to 2.981 W/(m·K), with an average of 2.16 W/(m·K). This limited data set from the shallow portion of the section at Atlantis Bank does not show any relation between rock type or alteration and thermal conductivity.

References

Adams, F.D., and Coker, E.G., 1906. An investigation into the elastic constants of rocks, more especially with reference to cubic compressibility. *American Journal of Science* (Series 4), 22(128):95–123. **http://dx.doi.org/10.2475/ajs.s4-22.128.95**

Adams, L.H., and Williamson, E.D., 1923. On the compressibility of minerals and rocks at high pressure. *Journal of the Franklin Institute,* 195(4):475–529. **http://dx.doi.org/10.1016/S0016-0032(23)90314-5**

Allerton, S., and Tivey, M.A., 2001. Magnetic polarity structure of the lower oceanic crust. *Geophysical Research Letters,* 28(3):423–426. **http://dx.doi.org/10.1029/2000GL008493**

Arai, S., Dick, H.J.B., and Scientific Party, 2000. *Cruise Report, Mode 2000* (*Kairei/Kaiko* KR00-06): Yokosuka, Japan (Japanese Agency for Marine-Earth Science and Technology).

Baines, A.G., Cheadle, M.J., Dick, H.J.B., Hosford Scheirer, A., John, B.E., Kusznir, N.J., and Matsumoto, T., 2003. Mechanism for generating the anomalous uplift of oceanic core complexes: Atlantis Bank, Southwest Indian Ridge. *Geology,* 31(12):1105–1108. **http://dx.doi.org/10.1130/G19829.1**

Baines, A.G., Cheadle, M.J., Dick, H.J.B., Hosford Scheirer, A., John, B.E., Kusznir, N.J., and Matsumoto, T., 2007. The evolution of the Southwest Indian Ridge from 55°45′E–62°E: changes in plate-boundary geometry since 26 Ma. *Geochemistry, Geophysics, Geosystems,* 8(6):Q06022. **http://dx.doi.org/10.1029/2006GC001559**

Baines, A.G., Cheadle, M.J., John, B.E., and Schwartz, J.J., 2008. The rate of oceanic detachment faulting at Atlantis Bank, SW Indian Ridge. *Earth and Planetary Science Letters,* 273(1–2):105–114. **http://dx.doi.org/10.1016/j.epsl.2008.06.013**

Biddle, J.F., Fitz-Gibbon, S., Schuster, S.C., Brenchley, J.E., and House, C.H., 2008. Metagenomic signatures of the Peru margin subseafloor biosphere show a genetically distinct environment. *Proceedings of the National Academy of Sciences of the United States of America,* 105(30):10583–10588. **http://dx.doi.org/10.1073/pnas.0709942105**

Blackman, D.K., Ildefonse, B., John, B.E., Ohara, Y., Miller, D.J., Abe, N., Abratis, M., Andal, E.S., Andreani, M., Awaji, S., Beard, J.S., Brunelli, D., Charney, A.B., Christie, D.M., Collins, J., Delacour, A.G., Delius, H., Drouin, M., Einaudi, F., Escartín, J. Frost, B.R., Früh-Green, G., Fryer, P.B., Gee, J.S., Godard, M., Grimes, C.B., Halfpenny, A., Hansen, H.-E., Harris, A.C., Tamura, A., Hayman, N.W., Hellebranc, E., Hirose, T., Hirth, J.G., Ishimaru, S., Johnson, K.T.M., Karner, G.D., Linek, M., MacLeod, C.J., Maeda, J., Mason, O.U., McCaig, A.M., Michibayashi, K., Morris, A., Nakagawa, T., Nozaka, T., Rosner, M., Searle, R.C., Suhr, G., Tominaga, M., von der Handt, A., Yamasaki, T., and Zhao, X., 2011. Drilling constraints on lithospheric accretion and evolution at Atlantis Massif, Mid-Atlantic Ridge, 30°N. *Journal of Geophysical Research: Solid Earth,* 116(B7):B07103. **http://dx.doi.org/10.1029/2010JB007931**

Blackman, D.K., Ildefonse, B., John, B.E., Ohara, Y., Miller, D.J., MacLeod, C.J., and the Expedition 304/305 Scientists, 2006. *Proceedings of the Integrated Ocean Drilling Program,* 304/305: College Station, TX (Integrated Ocean Drilling Program Management International, Inc.). **http://dx.doi.org/10.2204/iodp.proc.304305.2006**

Blumenfeld, P., and Bouchez, J.-L., 1988. Shear criteria in granite and migmatite deformed in the magmatic and solid states. *Journal of Structural Geology,* 10(4):361–372. **http://dx.doi.org/10.1016/0191-8141(88)90014-4**

Cann, J.R., Blackman, D.K., Smith, D.K., McAllister, E., Janssen, B., Mello, S., Avgerinos, E., Pascoe, A.R., and Escartin, J., 1997. Corrugated slip surfaces formed at ridge–transform intersections on the Mid-Atlantic Ridge. *Nature,* 385(6614):329–332. **http://dx.doi.org/10.1038/385329a0**

Cannat, M., Mével, C., and Stakes, D., 1991. Normal ductile shear zones at an oceanic spreading ridge: tectonic evolution of Site 735 gabbros (southwest Indian Ocean). *In* Von Herzen, R.P., Robinson, P.T., et al., *Proceedings of the Ocean Drilling Program, Scientific Results,* 118: College Station, TX (Ocean Drilling Program), 415–429. **http://dx.doi.org/10.2973/odp.proc.sr.118.157.1991**

Cannat, M., Sauter, D., Mendel, V., Ruellan, E., Okino, K., Escartin, J., Combier, V., and Baala, M., 2006. Modes of seafloor generation at a melt-poor ultraslow-spreading ridge. *Geology,* 34(7):605–608. **http://dx.doi.org/10.1130/G22486.1**

Casey, J.F., Banerji, D., and Zarian, P., 2007. Leg 179 synthesis: geochemistry, stratigraphy, and structure of gabbroic rocks drilled in ODP Hole 1105A, Southwest Indian Ridge. *In* Casey, J.F., and Miller, D.J. (Eds.), *Proceedings of the Ocean Drilling Program, Scientific Results,* 179: College Station, TX (Ocean Drilling Program), 1–125. **http://dx.doi.org/10.2973/odp.proc.sr.179.001.2007**

Cowen, J.P., Giovannoni, S.J., Kenig, F., Johnson, H.P., Butterfield, D., Rappé, M.S., Hutnak, M., and Lam, P., 2003. Fluids from aging ocean crust that support microbial life. *Science,* 299(5603):120–123. **http://dx.doi.org/10.1126/science.1075653**

Delacour, A., Früh-Green, G.L., Bernasconi, S.M., Schaeffer, P., and Kelley, D.S., 2008. Carbon geochemistry of serpentinites in the Lost City hydrothermal system (30°N, MAR). *Geochimica et Cosmochimica Acta,* 72(15):3681–3702. **http://dx.doi.org/10.1016/j.gca.2008.04.039**

Dick, H.J.B., Arai, S., Hirth, G., John, B.J., and KROO-06 Scientific Party, 2001. A subhorizontal cross-section through the crust mantle boundary at the SW Indian Ridge. *Geophysical Research Abstracts,* 3:794.

Dick, H.J.B., MacLeod, C.J., Robinson, P.T., Allerton, S., and Tivey, M.A., 1999. Bathymetry of Atlantis Bank—Atlantis II Fracture Zone: Southwest Indian Ridge. *In* Dick, H.J.B., Natland, J.H., Miller, D.J., et al., *Proceedings of the Ocean Drilling Program, Initial Reports,* 176: College Station, TX (Ocean Drilling Program), 1–13. **http://dx.doi.org/10.2973/odp.proc.ir.176.104.1999**

Dick, H.J.B., Meyer, P.S., Bloomer, S., Kirby, S., Stakes, D., and Mawer, C., 1991a. Lithostratigraphic evolution of an in-situ section of oceanic Layer 3. *In* Von Herzen, R.P., Robinson, P.T., et al., *Proceedings of the Ocean Drilling Program, Scientific Results,* 118: College Station, TX (Ocean Drilling Program), 439–538. **http://dx.doi.org/10.2973/odp.proc.sr.118.128.1991**

Dick, H.J.B., Natland, J.H., Alt, J.C., Bach, W., Bideau, D., Gee, J.S., Haggas, S., Hertogen, J.G.H., Hirth, G., Holm, P.M., Ildefonse, B., Iturrino, G.J., John, B.E., Kelley, D.S., Kikawa, E., Kingdon, A., LeRoux, P.J., Maeda, J., Meyer, P.S., Miller, D.J., Naslund, H.R., Niu, Y.-L., Robinson, P.T., Snow, J., Stephen, R.A., Trimby, P.W., Worm, H.-U., and Yoshinobu, A., 2000. A long in situ section of the lower ocean crust: results of ODP Leg 176 drilling at the Southwest Indian Ridge. *Earth and Planetary Science Letters,* 179(1):31–51. **http://dx.doi.org/10.1016/S0012-821X(00)00102-3**

Dick, H.J.B., Natland, J.H., and Ildefonse, B., 2006. Past and future impact of deep drilling in the oceanic crust and mantle. *Oceanography,* 19(4):72–80. **http://dx.doi.org/10.5670/oceanog.2006.06**

Dick, H.J.B., Natland, J.H., Miller, D.J., et al., 1999. *Proceedings of the Ocean Drilling Program, Initial Reports,* 176: College Station, TX (Ocean Drilling Program). **http://dx.doi.org/10.2973/odp.proc.ir.176.1999**

Dick, H.J.B., Ozawa, K., Meyer, P.S., Niu, Y., Robinson, P.T., Constantin, M., Hebert, R., Maeda, J., Natland, J.H., Hirth, J.G., and Mackie, S.M., 2002. Primary silicate mineral chemistry of a 1.5-km section of very slow spreading lower ocean crust: ODP Hole 735B, Southwest Indian Ridge. *In* Natland, J.H., Dick, H.J.B, Miller, D.J., and Von Herzen, R.P. (Eds.), *Proceedings of the Ocean Drilling Program, Scientific Results,* 176: College Station, TX (Ocean Drilling Program), 1–60. **http://dx.doi.org/10.2973/odp.proc.sr.176.001.2002**

Dick, H.J.B., Schouten, H., Meyer, P.S., Gallo, D.G., Bergh, H., Tyce, R., Patriat, P., Johnson, K.T.M., Snow, J., and Fisher, A., 1991b. Tectonic evolution of the Atlantis II Fracture Zone. *In* Von Herzen, R.P., Robinson, P.T., et al., *Proceedings of the Ocean Drilling Program, Scientific Results,* 118: College Station, TX (Ocean Drilling Program), 359–398. **http://dx.doi.org/10.2973/odp.proc.sr.118.156.1991**

Dick, H.J.B., Tivey, M.A., and Tucholke, B.E., 2008. Plutonic foundation of a slow-spreading ridge segment: oceanic core complex at Kane Megamullion, 23°30′N, 45°20′W. *Geochemistry, Geophysics, Geosystems,* 9(5):Q05014. **http://dx.doi.org/10.1029/2007GC001645**

Drouin, M., Godard, M., Ildefonse, B., Bruguier, O., and Garrido, C.J., 2009. Geochemical and petrographic evidence for magmatic impregnation in the oceanic lithosphere at Atlantis Massif, Mid-Atlantic Ridge (IODP Hole U1309D, 30°N). *Chemical Geology,* 264(1–4):71–88. **http://dx.doi.org/10.1016/j.chemgeo.2009.02.013**

Edgcomb, V.P., Beaudoin, D., Gast, R., Biddle, J.F., and Teske, A., 2011. Marine subsurface eukaryotes: the fungal majority. *Environmental Microbiology,* 13(1):172–183. **http://dx.doi.org/10.1111/j.1462-2920.2010.02318.x**

Escartín, J., Mével, C., MacLeod, C.J., and McCaig, A.M., 2003. Constraints on deformation conditions and the origin of oceanic detachments: the Mid-Atlantic Ridge core complex at 15°45′N. *Geochemistry, Geophysics, Geosystems,* 4(8):1067. **http://dx.doi.org/10.1029/2002GC000472**

Expedition 304/305 Scientists, 2006. Expedition 304/305 summary. *In* Blackman, D.K., Ildefonse, B., John, B.E., Ohara, Y., Miller, D.J., MacLeod, C.J., and the Expedition 304/305 Scientists, *Proceedings of the Integrated Ocean Drilling Program,* 304/305: College Station, TX (Integrated Ocean

Drilling Program Management International, Inc.). **http://dx.doi.org/10.2204/iodp.proc.304305.101.2006**

Fisher, R.L., and Sclater, J.G., 1983. Tectonic evolution of the southwest Indian Ocean since the mid-Cretaceous: plate motions and stability of the pole of Antarctica/Africa for at least 80 Myr. *Geophysical Journal International,* 73(2):553–576. **http://dx.doi.org/10.1111/j.1365-246X.1983.tb03330.x**

Fisk, M.R., Giovannoni, S.J., and Thorseth, I.H., 1998. Alteration of oceanic volcanic glass: textural evidence of microbial activity. *Science,* 281(5379):978–980. **http://dx.doi.org/10.1126/science.281.5379.978**

Gillis, K.M., Snow, J.E., Klaus, A., Abe, N., Adrião, Á.B., Akizawa, N., Ceuleneer, G., Cheadle, M.J., Faak, K., Falloon, T.J., Friedman, S.A., Godard, M., Guerin, G., Harigane, Y., Horst, A.J., Hoshide, T., Ildefonse, B., Jean, M.M., John, B.E., Koepke, J., Machi, S., Maeda, J., Marks, N.E., McCaig, A.M., Meyer, R., Morris, A., Nozaka, T., Python, M., Saha, A., and Wintsch, R.P., 2014. Primitive layered gabbros from fast-spreading lower oceanic crust. *Nature,* 505(7482):204–207. **http://dx.doi.org/10.1038/nature12778**

Godard, M., Awaji, S., Hansen, H., Hellebrand, E., Brunelli, D., Johnson, K., Yamasaki, T., Maeda, J., Abratis, M., Christie, D., Kato, Y., Mariet, C., and Rosner, M., 2009. Geochemistry of a long in-situ section of intrusive slow-spread oceanic lithosphere: results from IODP Site U1309 (Atlantis Massif, 30°N Mid-Atlantic-Ridge). *Earth and Planetary Science Letters,* 279(1–2):110–122. **http://dx.doi.org/10.1016/j.epsl.2008.12.034**

Gradstein, F.M., Ogg, J.G., Schmitz, M.D., and Ogg, G.M. (Eds.), 2012. *The Geological Time Scale 2012:* Amsterdam (Elsevier).

Handy, M., Hirth, G., and Burgmann, R., 2007. Continental fault structure and rheology from the frictional-to-viscous transition downward. *In* Handy, M., Hirth, G., and Hovius, N. (Eds.), *Tectonic Faults: Agents of Change on a Dynamic Earth (Dahlem Workshop Reports):* Cambridge, MA (The MIT Press), 139–181.

Hess, H.H., 1960. The evolution of ocean basins. *In* Hill, M.N., Goldberg, E., Munk, W., and Iselin, O.D. (Eds.), *The Sea, Ideas and Observations:* New York (Interscience Publishers), 1–38.

Hess, H.H., 1962. History of ocean basins. *In* Engel, A.E.J., et al. (Eds.), *Petrological Studies: A Volume in Honor of A.F. Buddington:* Boulder, CO (Geological Society of America), 599–620. **http://dx.doi.org/10.1130/Petrologic.1962.599**

Hosford, A., Tivey, M., Matsumoto, T., Dick, H., Schouten, H., and Kinoshita, H., 2003. Crustal magnetization and accretion at the Southwest Indian Ridge near the Atlantis II Fracture Zone, 0–25 Ma. *Journal of Geophysical Research: Solid Earth,* 108(B3):2169. **http://dx.doi.org/10.1029/2001JB000604**

Inagaki, F., Hinrichs, K.-U., Kubo, Y., Bowles, M.W., Heuer, V.B., Long, W.-L., Hoshino, T., Ijiri, A., Imachi, H., Ito, M., Kaneko, M., Lever, M.A., Lin, Y.-S., Methé, B.A., Morita, S., Morono, Y., Tanikawa, W., Bihan, M., Bowden, S.A., Elvert, M., Glombitza, C., Gross, D., Harrington, G.J., Hori, T., Li, K., Limmer, D., Liu, C.-H., Murayama, M., Ohkouchi, N., Ono, S., Park, Y.-S., Phillips, S.C., Prieto-Mollar, X., Purkey, M., Riedinger, N., Sanada, Y., Sauvage, J., Snyder, G., Susilawati, R., Takano, Y., Tasumi, E., Terada, T., Tomaru, H., Trembath-Reichert, E., Wang, D.T., and Yamada, Y., 2015. Exploring deep microbial life in coal-bearing sediment down to ~2.5 km below the ocean floor. *Science,* 349(6246):420–424. **http://dx.doi.org/10.1126/science.aaa6882**

Inagaki, F., Nunoura, T., Nakagawa, S., Teske, A., Lever, M., Lauer, A., Suzuki, M., Takai, K., Delwiche, M., Colwell, F.S., Nealson, K.H., Horikoshi, K., D'Hondt, S., and Jørgensen, B.B., 2006. Biogeographical distribution and diversity of microbes in methane hydrate-bearing deep marine sediments on the Pacific Ocean margin. *Proceedings of the National Academy of Sciences of the United States of America,* 103(8):2815–2820. **http://dx.doi.org/10.1073/pnas.0511033103**

Jungbluth, S.P., Grote, J., Lin, H.-T., Cowen, J.P., and Rappé, M.S., 2013. Microbial diversity within basement fluids of the sediment-buried Juan de Fuca Ridge flank. *The ISME Journal,* 7:161–172. **http://dx.doi.org/10.1038/ismej.2012.73**

Kikawa, E., and Pariso, J.E., 1991. Magnetic properties of gabbros from Hole 735B, Southwest Indian Ridge. *In* Von Herzen, R.P., Robinson, P.T., et al., *Proceedings of the Ocean Drilling Program, Scientific Results,* 118: College Station, TX (Ocean Drilling Program), 285–307. **http://dx.doi.org/10.2973/odp.proc.sr.118.148.1991**

Kinoshita, H., Dick, H.J.B., and Shipboard Scientific Party, 2001. *Atlantis II Fracture Zone: MODE'98 Preliminary Report:* Yokosuka, Japan (JAMSTEC Deep Sea Research).

Kinoshita, J., Dick, H., and Shipboard Party JAMSTEC/WHOI, 1999. Deep sea diving expedition in SW Indian Ridge (paper presented in honor of Don Heinrichs for his dedication in Marine Geosciences of NSF), *Eos, Transactions of the American Geophysical Union,* 80(46):F526.

Koepke, J., Feig, S.T., Snow, J., and Freise, M., 2004. Petrogenesis of oceanic plagiogranites by partial melting of gabbros: an experimental study. *Contributions to Mineralogy and Petrology,* 146(4):414–432. **http://dx.doi.org/10.1007/s00410-003-0511-9**

Lavier, L., Buck, W.R., and Poliakov, A.N.B., 1999. Self-consistent rolling-hinge model for the evolution of large-offset low-angle normal faults. *Geology,* 27(12):1127–1130. **http://dx.doi.org/10.1130/0091-7613(1999)027<1127:SCRHMF>2.3.CO;2**

Lever, M.A., Rouxel, O., Alt, J.C., Shimizu, N., Ono, S., Coggon, R.M., Shanks, W.C., III, Laphan, L., Elvert, M., Prieto-Mollar, X., Hinrichs, K.-U., Inagaki, F., and Teske, A., 2013. Evidence for microbial carbon and sulfur cycling in deeply buried ridge flank basalt. *Science,* 339(6125):1305–1308. **http://dx.doi.org/10.1126/science.1229240**

Lissenberg, C.J., MacLeod, C.J., Howard, K.A., and Godard, M., 2013. Pervasive reactive melt migration through fast-spreading lower oceanic crust (Hess Deep, equatorial Pacific Ocean). *Earth and Planetary Science Letters,* 361:436–447. **http://dx.doi.org/10.1016/j.epsl.2012.11.012**

MacLeod, C.J., Dick, H.J.B., Allerton, S., Robinson, P.T., Coogan, L.A., Edwards, S.J., Galley, A., Gillis, K.M., Hirth, G., Hunter, A.G., Hutchinson, D., Kvassnes, A.J., Natland, J.H., Salisbury, M., Schandl, E.S., Stakes, D.S., Thompson, G.M., and Tivey, M.A., 1998. Geological mapping of slow-spread lower ocean crust: a deep-towed video and wireline rock drilling survey of Atlantis Bank (ODP Site 735, SW Indian Ridge). *InterRidge News,* 7(2):39–43.

MacLeod, C.J., Dick, H.J.B., Blum, P., Abe, N., Blackman, D.K., Bowles, J.A., Cheadle, M.J., Cho, K., Ciążela, J., Deans, J.R., Edgcomb, V.P., Ferrando, C., France, L., Ghosh, B., Ildefonse, B.M., Kendrick, M.A., Koepke, J.H., Leong, J.A.M., Liu, C., Ma, Q., Morishita, T., Morris, A., Natland, J.H., Nozaka, T., Pluemper, O., Sanfilippo, A., Sylvan, J.B., Tivey, M.A., Tribuzio, R., and Viegas, L.G.F., 2017a. Hole 1105A redescription. *In* MacLeod, C.J., Dick, H.J.B., Blum, P., and the Expedition 360 Scientists, *Southwest Indian Ridge Lower Crust and Moho.* Proceedings of the International Ocean Discovery Program, 360: College Station, TX (International Ocean Discovery Program). **http://dx.doi.org/10.14379/iodp.proc.360.104.2017**

MacLeod, C.J., Dick, H.J.B., Blum, P., Abe, N., Blackman, D.K., Bowles, J.A., Cheadle, M.J., Cho, K., Ciążela, J., Deans, J.R., Edgcomb, V.P., Ferrando, C., France, L., Ghosh, B., Ildefonse, B.M., Kendrick, M.A., Koepke, J.H., Leong, J.A.M., Liu, C., Ma, Q., Morishita, T., Morris, A., Natland, J.H., Nozaka, T., Pluemper, O., Sanfilippo, A., Sylvan, J.B., Tivey, M.A., Tribuzio, R., and Viegas, L.G.F., 2017b. Site U1473. *In* MacLeod, C.J., Dick, H.J.B., Blum, P., and the Expedition 360 Scientists, *Southwest Indian Ridge Lower Crust and Moho.* Proceedings of the International Ocean Discovery Program, 360: College Station, TX (International Ocean Discovery Program). **http://dx.doi.org/10.14379/iodp.proc.360.103.2017**

MacLeod, C.J., Escartin, J., Banerji, D., Banks, G.J., Gleeson, M., Irving, D.H.B., Lilly, R.M., McCaig, A.M., Niu, Y., Allerton, S., and Smith, D.K., 2002. Direct geological evidence for oceanic detachment faulting: the Mid-Atlantic Ridge, 15°45′N. *Geology,* 30(10):879–882. **http://dx.doi.org/10.1130/0091-7613(2002)030<0879:DGEFOD>2.0.CO;2**

MacLeod, C.J., Searle, R.C., Murton, B.J., Casey, J.F., Mallows, C., Unsworth, S.C., Achenbach, K.L., and Harris, M., 2009. Life cycle of oceanic core complexes. *Earth and Planetary Science Letters,* 287(3–4):333–344. **http://dx.doi.org/10.1016/j.epsl.2009.08.016**

MacLeod, C.J., Wright, W.P., Perry, C.T., and Dick, H.J.B., 2000. Tectonic evolution and uplift/subsidence history of Atlantis Bank, a Transverse Ridge near the Atlantis II Fracture Zone, SW Indian Ridge. *Eos, Transactions of the American Geophysical Union,* 81:1129.

Mason, O.U., Nakagawa, T., Rosner, M., Van Nostrand, J.D., Zhou, J., Maruyama, A., Fisk, M.R., and Giovannoni, S.J., 2010. First investigation of the microbiology of the deepest layer of ocean crust. *PLoS One,* 5(11):e15399. **http://dx.doi.org/10.1371/journal.pone.0015399**

Matsumoto, T., Dick, H.J.B., and Scientific Party, 2002. *Investigation of Atlantis Bank and the SW Indian Ridge from 568E to 588E: Preliminary Report:* Tokyo (Japanese Agency for Marine-Earth Science and Technology).

Mendel, V., Sauter, D., Parson, L., and Vanney, J.-R., 1997. Segmentation and morphotectonic variations along a super slow-spreading center: the Southwest Indian Ridge (57° E–70° E). *Marine Geophysical Research,* 19(6):505–533. **http://dx.doi.org/10.1023/A:1004232506333**

Mendel, V., Sauter, D., Rommevaux-Jestin, C., Patriat, P., Lefebvre, F., and Parson, L.M., 2003. Magmato-tectonic cyclicity at the ultra-slow spreading Southwest Indian Ridge: evidence from variations of axial volcanic ridge morphology and abyssal hills pattern. *Geochemistry, Geophysics, Geosystems,* 4(5):9102. **http://dx.doi.org/10.1029/2002GC000417**

Ménez, B., Pasini V., and Brunelli, D., 2012. Life in the hydrated suboceanic mantle. *Nature Geoscience,* 5(2):133–137. **http://dx.doi.org/10.1038/ngeo1359**

Miller, D.J., and Christensen, N.I., 1997. Seismic velocities of lower crustal and upper mantle rocks from the slow-spreading Mid-Atlantic Ridge, south of the Kane Transform Zone (MARK). *In* Karson, J.A., Cannat, M., Miller, D.J., and Elthon, D. (Eds.), *Proceedings of the Ocean Drilling Program, Scientific Results,* 153: College Station, TX (Ocean Drilling Program), 437–454. **http://dx.doi.org/10.2973/odp.proc.sr.153.043.1997**

Minshull, T.A., Muller, M.R., Robinson, C.J., White, R.S., and Bickle, M.J., 1998. Is the oceanic Moho a serpentinization front? *In* Mills, R.A., and Harrison, K. (Eds.), *Modern Ocean Floor Processes and the Geological Record.* Geological Society Special Publications, 148(1):71–80. **http://dx.doi.org/10.1144/GSL.SP.1998.148.01.05**

Miranda, E.A., and John, B.E., 2010. Strain localization along the Atlantis Bank oceanic detachment fault system, Southwest Indian Ridge. *Geochemistry, Geophysics, Geosystems,* 11(4):Q04002. **http://dx.doi.org/10.1029/2009GC002646**

Muller, M.R., Minshull, T.A., and White, R.S., 2000. Crustal structure of the Southwest Indian Ridge at the Atlantis II Fracture Zone. *Journal of Geophysical Research: Solid Earth,* 105(B11):25809–25828. **http://dx.doi.org/10.1029/2000JB900262**

Muller, M.R., Robinson, C.J., Minshull, T.A., White, R.S., and Bickle, M.J., 1997. Thin crust beneath Ocean Drilling Program Borehole 735B at the Southwest Indian Ridge? *Earth and Planetary Science Letters,* 148(1–2):93–107. **http://dx.doi.org/10.1016/S0012-821X(97)00030-7**

Mutter, J.C., and Karson, J.A., 1992. Structural processes at slow-spreading ridges. *Science,* 257(5070):627–634. **http://dx.doi.org/10.1126/science.257.5070.627**

Natland, J.H., and Dick, H.J.B., 2001. Formation of the lower ocean crust and the crystallization of gabbroic cumulates at a very slowly spreading ridge. *Journal of Volcanology and Geothermal Research,* 110(3–4):191–233. **http://dx.doi.org/10.1016/S0377-0273(01)00211-6**

Natland, J.H., and Dick, H.J.B., 2002. Stratigraphy and composition of gabbros drilled in Ocean Drilling Program Hole 735B, Southwest Indian Ridge: a synthesis of geochemical data. *In* Natland, J.H., Dick, H.J.B., Miller, D.J., and Von Herzen, R.P. (Eds.), *Proceedings of the Ocean Drilling Program, Scientific Results,* 176: College Station, TX (Ocean Drilling Program), 1–69. **http://dx.doi.org/10.2973/odp.proc.sr.176.002.2002**

Natland, J.H., Meyer, P.S., Dick, H.J.B., and Bloomer, S.H., 1991. Magmatic oxides and sulfides in gabbroic rocks from Hole 735B and the later development of the liquid line of descent. *In* Von Herzen, R.P., Robinson, P.T., et al., *Proceedings of the Ocean Drilling Program, Scientific Results,* 118: College Station, TX (Ocean Drilling Program), 75–111. **http://dx.doi.org/10.2973/odp.proc.sr.118.163.1991**

Orcutt, B.N., Wheat, C.G., Rouxel, O., Hulme, S., Edwards, K.J., and Bach, W., 2013. Oxygen consumption rates in subseafloor basaltic crust derived from a reaction transport model. *Nature Communications,* 4:2539. **http://dx.doi.org/10.1038/ncomms3539**

Orsi, W., Biddle, J.F., and Edgcomb, V., 2013a. Deep sequencing of subseafloor eukaryotic rRNA reveals active fungi across marine subsurface provinces. *PLoS ONE,* 8(2):e56335. **http://dx.doi.org/10.1371/journal.pone.0056335**

Orsi, W.D., Edgcomb, V.P., Christman, G.D., and Biddle, J.F., 2013b. Gene expression in the deep biosphere. *Nature,* 499(7457):205–208. **http://dx.doi.org/10.1038/nature12230**

Palmiotto, C., Corda, L., Ligi, M., Cipriani, A., Dick, H.J.B., Douville, E., Gasperini, L., Montagna, P., Thil, F., Borsetti, A.M., Balestra, B., and Bonatti, E., 2013. Nonvolcanic tectonic islands in ancient and modern oceans. *Geochemistry, Geophysics, Geosystems,* 14(10):4698–4717. **http://dx.doi.org/10.1002/ggge.20279**

Parkes, R.J., Cragg, B.A., Bale, S.J., Getliff, J.M., Goodman, K., Rochelle, P.A., Fry, J.C., Weightman, A.J., and Harvey, S.M., 1994. Deep bacterial biosphere in Pacific Ocean sediments. *Nature,* 371(6496):410–413. **http://dx.doi.org/10.1038/371410a0**

Pettigrew, T.L., Casey, J.F., Miller, D.J., et al., 1999. *Proceedings of the Ocean Drilling Program, Initial Reports,* 179: College Station, TX (Ocean Drilling Program). **http://dx.doi.org/10.2973/odp.proc.ir.179.1999**

Proskurowski, G., Lilley, M.D., Seewald, J.S., Früh-Green, G.L., Olson, E.J., Lupton, J.E., Sylva, S.P., and Kelley, D.S., 2008. Abiogenic hydrocarbon production at Lost City hydrothermal field. *Science,* 319(5863):604–607. **http://dx.doi.org/10.1126/science.1151194**

Robinson, C.J., White, R.S., Bickle, M.J., and Minshull, T.A., 1996. Restricted melting under the very slow-spreading Southwest Indian Ridge. *Geological Society Special Publication,* 118(1):131–141. **http://dx.doi.org/10.1144/GSL.SP.1996.118.01.07**

Robinson, P.T., Von Herzen, R., et al., 1989. *Proceedings of the Ocean Drilling Program, Initial Reports,* 118: College Station, TX (Ocean Drilling Program). **http://dx.doi.org/10.2973/odp.proc.ir.118.1989**

Sauter, D., Cannat, M., Rouméjon, S., Andreani, M., Birot, D., Bronner, A., Brunelli, D., Carlut, J., Delacour, A., Guyader, V., MacLeod, C.J., Manatschal, G., Mendel, V., Ménez, B., Pasini, V., Ruellan, E., and Searle, R., 2013. Continuous exhumation of mantle-derived rocks at the Southwest Indian Ridge for 11 million years. *Nature Geoscience,* 6(4):314–320. **http://dx.doi.org/10.1038/ngeo1771**

Sauter, D., Carton, H., Mendel, V., Munschy, M., Rommevaux-Jestin, C., Schott, J.-J., and Whitechurch, H., 2004. Ridge segmentation and the magnetic structure of the Southwest Indian Ridge (at 50°30′E, 55°30′E, and 66°20′E): implications for magmatic processes at ultraslow-spreading centers. *Geochemistry, Geophysics, Geosystems,* 5(5):Q05K08. **http://dx.doi.org/10.1029/2003GC000581**

Schroeder, T., and John, B.E., 2004. Strain localization on an oceanic detachment fault system, Atlantis Massif, 30°N, Mid-Atlantic Ridge. *Geochemistry, Geophysics, Geosystems,* 5:Q11007. **http://dx.doi.org/10.1029/2004GC000728**

Shock, E.L., 2009. Minerals as energy sources for microorganisms. *Economic Geology,* 104(8):1235–1248. **http://dx.doi.org/10.2113/gsecongeo.104.8.1235**

Smith, D.K., Cann, J.R., and Escartin, J., 2006. Widespread active detachment faulting and core complex formation near 13°N on the Mid-Atlantic Ridge. *Nature,* 442(7101):440–443. **http://dx.doi.org/10.1038/nature04950**

Sylvan, J.B., Hoffman, C.L., Momper, L.M., Toner, B.M., Amend, J.P., and Edwards, K.J., 2015. *Bacillus rigiliprofundi* sp. nov., an endospore-forming, Mn-oxidizing, moderately halophilic bacterium isolated from deep subseafloor basaltic crust. *International Journal of Systematic and Evolutionary Microbiology,* 65:1992–1998. **http://dx.doi.org/10.1099/ijs.0.000211**

Till, J.L., and Moskowitz, B., 2013. Magnetite deformation mechanism maps for better prediction of strain partitioning. *Geophysical Research Letters,* 40(4):697–702. **http://dx.doi.org/10.1002/grl.50170**

Tucholke, B.E., Lin, J., and Kleinrock, M.C., 1998. Megamullions and mullion structure defining oceanic metamorphic core complexes on the Mid-Atlantic Ridge. *Journal of Geophysical Research: Solid Earth,* 103(B5):9857–9866. **http://dx.doi.org/10.1029/98JB00167**

Wrinch, D., and Jeffreys, H., 1923. On the seismic waves from the Oppau explosion of 1921 Sept. 21. *Geophysical Journal International,* 1(Supplement s2):15–22. **http://dx.doi.org/10.1111/j.1365-246X.1923.tb06565.x**